Supporting Information

Highly Phosphorescent Dimers of $PtAu_2$ Complexes and the Use in Solution-Processed OLEDs

Da-Sheng Zheng, Ming Yang, Jin-Yun Wang, and Zhong-Ning Chen*

Corresponding Author
Zhong-Ning Chen−*College of Chemistry and Material Science, Fujian Normal University, Fuzhou, Fujian, 350007, China; State Key Laboratory of Structural Chemistry, Fujian Institute of Research on the Structure of Matter, Chinese Academy of Sciences, Fuzhou, Fujian 350002, China; Fujian Science & Technology Innovation Laboratory for Optoelectronic Information of China, Fuzhou, Fujian 350108, China; orcid.org/0000-0003-3589-3745; Email: czn@fjirsm.ac.cn*

Authors
Da-Sheng Zheng−*College of Chemistry and Material Science, Fujian Normal University, Fuzhou, Fujian, 350007, China; State Key Laboratory of Structural Chemistry, Fujian Institute of Research on the Structure of Matter, Chinese Academy of Sciences, Fuzhou, Fujian 350002, China*

Ming Yang−*State Key Laboratory of Structural Chemistry, Fujian Institute of Research on the Structure of Matter, Chinese Academy of Sciences, Fuzhou, Fujian 350002, China*

Jin-Yun Wang−*State Key Laboratory of Structural Chemistry, Fujian Institute of Research on the Structure of Matter, Chinese Academy of Sciences, Fuzhou, Fujian 350002, China*

Experimental Section

All the reactions were conducted under dry argon using Schlenk technique and vacuum-line system. All solvents were dried and distilled from appropriate drying agents prior to use. Bis(di-o-tolylphosphino-methyl)phenylphosphine (dTolmp)[1] were prepared by synthetic procedures described in literature.

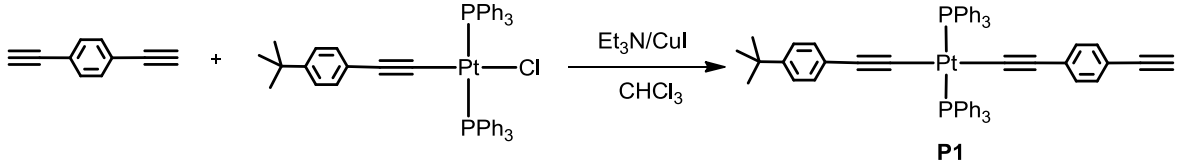

P1

Synthesis of P1. To a Schlenk flask were added 1,4-diethynylbenzene (125 mg, 1 mmol), CuI (1 mg) and dry $CHCl_3$ (50 mL) with stirring for 0.5 h. Then a dry $CHCl_3$ (30 mL) solution containing $Pt(PPh_3)_2(C{\equiv}CC_6H_4Bu^t\text{-}4)Cl$ (912 mg, 1 mmol) and Et_3N (0.1 mL, 1 mmol) was slowly added to the above Schlenk flask. After the mixed solution was stirred at 40 ℃ for 12 h, it was evaporated to dryness under reduced pressure. The product **P1** was purified by silica gel column chromatography using CH_2Cl_2-petroleum ether (v/v = 1 : 3) as eluent. Yield: 73%. ^{1}H NMR ($CDCl_3$, ppm): 7.80 (m, 12H), 7.45 – 7.31 (m, 18H), 7.05 (d, *J* = 8.3 Hz, 2H), 6.92 (d, *J* = 8.4 Hz, 2H), 6.23 (d, *J* = 8.3 Hz, 2H), 6.18 (d, *J* = 8.4 Hz, 2H), 3.02 (s, 1H, C≡C*H*), 1.18 (s, 9H, C_4H_9). ^{31}P NMR (162 MHz, $CDCl_3$, ppm): 18.7 (s, 1P, $J_{Pt\text{-}P}$ = 2645 Hz).

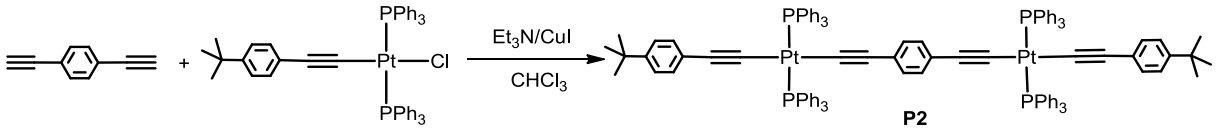

P2

Synthesis of P2. To a Schlenk flask were added 1,4-diethynylbenzene (50 mg, 0.4 mmol), CuI (1 mg) and dry $CHCl_3$ (20 mL) with stirring for 0.5 h. Then a dry $CHCl_3$ (20 mL) solution contianing $Pt(PPh_3)_2(C{\equiv}CC_6H_4Bu^t\text{-}4)Cl$ (728 mg, 0.8 mmol) and Et_3N (2 mL) was slowly added to the above Schlenk flask. After the mixed solution was stirred at 60 ℃ for 12 h, it was evaporated to dryness under reduced pressure. The product **P2** was purified by silica gel column chromatography using CH_2Cl_2-petroleum ether (v/v = 1 : 3) as eluent. Yield: 82%. ^{1}H NMR ($CDCl_3$, ppm): 7.78 (dd, *J* = 12.4, 5.8 Hz, 24H), 7.45 – 7.31 (m, 36H), 6.90 (d, *J* = 8.5

Hz, 4H), 6.14 (d, J = 8.4 Hz, 4H), 5.89 (s, 4H), 1.17 (s, 18H, C_4H_9). ^{31}P NMR (162 MHz, $CDCl_3$, ppm): 18.5 (s, 2P, $J_{Pt\text{-}P}$ = 2645 Hz).

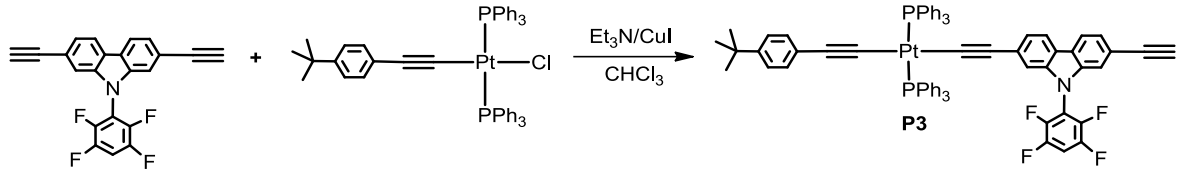

Synthesis of P3. This compound was prepared by the same synthetic procedure as that of **P1** except for using 2,7-diethynyl-9-(2,3,5,6-tetrafluorophenyl)-9H-carbazole in place of 1,4-diethynylbenzene. Yield: 76%. ^{1}H NMR ($CDCl_3$, ppm): 7.88 (d, J = 8.1 Hz, 1H), 7.85 – 7.76 (m, 12H), 7.05 (d, J = 8.3 Hz, 2H), 7.41 – 7.37 (m, 1H), 7.37 – 7.29 (m, 19H), 7.15 (s, 1H), 6.91 (d, J = 8.4 Hz, 2H), 6.31 (dd, J = 8.1, 1.0 Hz, 1H), 6.16 (d, J = 8.4 Hz, 2H), 6.07 (s, 1H), 3.09 (s, 1H, C≡C*H*), 1.18 (s, 9H, C_4H_9). ^{31}P NMR (162 MHz, $CDCl_3$, ppm): 18.7 (s, 1P, $J_{Pt\text{-}P}$ = 2645 Hz).

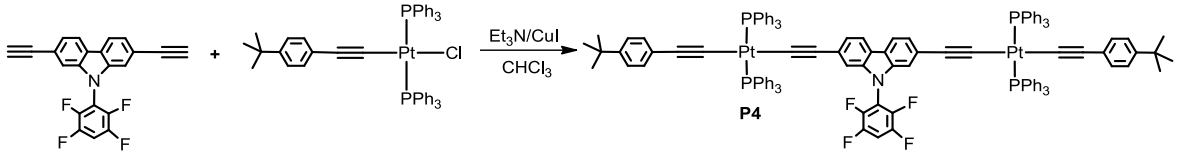

Synthesis of P4. This compound was prepared by the same synthetic procedure as that of **P2** except for using 2,7-diethynyl-9-(2,3,5,6-tetrafluorophenyl)-9H-carbazole in place of 1,4-diethynylbenzene. Yield: 87%. ^{1}H NMR ($CDCl_3$, ppm): 7.79 (d, J = 5.8 Hz, 24H), 7.49 (d, J = 8.0 Hz, 2H), 7.37 – 7.29 (m, 37H), 6.90 (d, J = 7.5 Hz, 4H), 6.23 (d, J = 8.1 Hz, 2H), 6.15 (d, J = 7.5 Hz, 4H), 5.96 (s, 1H), 1.17 (s, 18H, C_4H_9). ^{31}P NMR (162 MHz, $CDCl_3$, ppm): 18.6 (s, 2P, $J_{Pt\text{-}P}$ = 2649 Hz).

Physical Measurements. The ^{1}H and ^{31}P NMR spectra were performed on a Bruker Avance III (400 MHz) and ECZ600R (600 MHz) spectrometer with $SiMe_4$ as the internal reference and H_3PO_4 as the external reference, respectively. Splitting patterns are designated as singlet (s), doublet (d), and triplet (t). Splitting patterns that could not be interpreted or easily visualized are designated as multiplet (m) and broad (br). The UV-Vis absorption spectra were measured on a Perkin-Elmer Lambda 35 UV-Vis spectrophotometer using a 10 mm path quartz cell. The

high-resolution mass spectrometry (HRMS) was conducted on an Impact II mass spectrometer using dichloromethane and methanol mixtures as mobile phases. Cyclic voltammetry was performed with a CH Instruments Model CHI620E (CH Instruments, Inc.). The emission and excitation spectra together with the emissive lifetimes were measured on Edinburgh FLS-920 fluorescence spectrometer. The emission spectra and quantum yields were measured upon excitation at 380 nm. The luminescent lifetimes were conducted upon excitation at 375 nm by a laser source. The luminescent quantum yields (Φ_{em}) were determined by the integrating sphere (142 mm in diameter) using Edinburgh FLS-920 fluorescence spectrometer.

Crystal Structural Determination. X-ray single-crystal diffraction data were collected on a Bruker D8 Venture diffractometer using IμS 3.0 microfocus source Mo-Kα radiation (λ = 0.71073 Å) and PHOTON II CPAD detector. Frames were integrated with the Bruker SAINT software package (V8.38A) using a SAINT algorithm. Data were corrected for absorption effects using the multi-scan method (SADABS).[2] The single crystals X-ray diffraction for complex **2** was carried out on micro-focus metaljet diffractometer using Ga Kα radiation (λ = 1.3405 Å). And data reduction was performed with the CrysAlisPro package, at last analytical absorption correction was performed. All the structures were solved and refined using the Bruker SHELXTL Software Package, a computer program for automatic solution of crystal structures, and refined by the full-matrix least-squares method with ShelXle Version 4.8.6, a Qt graphical user interface for the SHELXL.[3]

Theoretical Computational Details. To understand the electronic and spectroscopic properties, the calculations were implemented by using Gaussian 16 program package[4] for complexes **1**–**4**. The geometrical structures as isolated molecules in the ground state and the lowest-energy triplet state were firstly optimized by density functional theory (DFT) method with the gradient corrected correlation functional PBE1PBE.[5] Then, in order to analyze the spectroscopic properties, 60 singlet and 6 triplet excited-states were calculated, respectively, based on the optimized structures in the ground state and lowest-energy triplet state to determine

the vertical excitation energies by time-dependent density functional theory (TD-DFT)[6-8] with the same functional used in the optimization process. In the calculation of excited states, the polarizable continuum model method (PCM)[9,10] with CH_2Cl_2 as solvent was employed. In these calculations, the Stuttgart-Dresden (SDD)[11] basis set and the effective core potentials (ECPs) were used to describe the Pt and Au atoms, while other non-metal atoms (P, N, F, C and H) were described by the all-electron basis set of 6-31G**. Visualization of the frontier molecular orbitals in the transition processes were performed by GaussView. The partial molecular orbital compositions were analyzed by the Ros&Schuit method[12] (C-squared population analysis method, SCPA) in Multiwfn 3.3.8 program.[13]

Table S1. Crystallographic Data of Complexes **1**·2CH_2Cl_2, **2** and **3**.

	1·2CH_2Cl_2	**2**	**3**
empirical formula	$C_{98}H_{96}Au_2Cl_4F_6O_6P_6PtS_2$	$C_{182}H_{178}Au_4F_{12}O_{12}P_{12}Pt_2S_4$	$C_{108}H_{95}Au_2F_{10}NO_6P_6PtS_2$
formula weight	2464.51	4463.16	2531.81
crystal system	Triclinic	Triclinic	Triclinic
space group	$P\ \bar{1}$	$P\ \bar{1}$	$P\ \bar{1}$
a (Å)	12.5423(6)	17.4884(8)	19.7599(15)
b (Å)	14.0963(7)	22.9913(10)	21.8031(17)
c (Å)	14.8713(7)	24.6512(10)	27.455(2)
α (deg)	113.020(2)	90.944(3)	101.252(3)
β (deg)	90.361(2)	102.973(4)	109.514(2)
γ (deg)	95.260(2)	100.813(4)	90.139(3)
V (Å^3)	2407.1(2)	9469.5(7)	10905.4(15)
Z	1	2	4
F (000)	1212.0	4380.0	4984.0
ρ_{calcd} (g/cm^3)	1.700	1.565	1.542
μ (mm^{-1})	4.808	7.013	4.158
Radiation (λ, Å)	0.71073	1.34139	0.71073
temperature (K)	150 K	293 K	150 K
GOF	1.137	1.028	1.053
R1 (F_o)[a]	0.0300(7956)	0.1549(26428)	0.1011(28116)
*w*R2 (F_o^2)[b]	0.0876(8732)	0.4276(38956)	0.2895(39813)

[a] $R1 = \Sigma|F_o-F_c|/\Sigma F_o$, [b] $wR2 = \Sigma[w(F_o^2-F_c^2)^2]/\Sigma[w(F_o)^2)]^{1/2}$

Table S2. The Partial Molecular Orbital Compositions (%) by SCPA Approach in the Ground State and the Absorption Transitions for Complex **1** in the CH_2Cl_2 Solution Calculated by TD-DFT Method at the PBE1PBE Level.

orbital	energy (eV)	MO contribution (%)				
		Pt (s/p/d)	Au (s/p/d)	dTolmp	$[C{\equiv}CC_6H_4Bu^t\text{-}4]^-$	$[C{\equiv}CC_6H_4C{\equiv}CH]^-$
LUMO+10	-1.17	28.36 (81/0/19)	18.34 (85/8/7)	51.49	1.04	0.76
LUMO+9	-1.29	18.25 (85/11/5)	17.56 (66/22/12)	59.35	0.52	4.33
LUMO+7	-1.39	16.29 (24/71/5)	7.03 (36/48/15)	64.61	1.30	10.76
LUMO+5	-1.49	11.14 (64/27/8)	12.35 (62/28/10)	69.96	1.93	4.62
LUMO+4	-1.50	24.05 (89/7/5)	14.13 (72/23/5)	56.57	0.98	4.26
LUMO+2	-1.66	7.49 (6/81/13)	23.62 (60/37/2)	67.41	1.00	0.48
LUMO+1	-1.68	9.63 (53/16/32)	18.41 (56/41/3)	60.57	0.64	10.75
LUMO	-2.56	10.25 (2/97/1)	16.23 (45/38/17)	60.30	5.12	8.10
HOMO	-6.24	22.59 (10/0/89)	2.14 (48/16/36)	3.02	41.52	30.74
HOMO-1	-6.66	5.48 (22/17/61)	14.60 (45/8/47)	10.64	30.44	38.84
HOMO-2	-6.67	33.10 (26/0/74)	38.44 (37/12/51)	24.69	1.31	2.46

state	*E*, nm (eV)	O.S.	transition (contrib.)	assignment	measured (nm)
S_1	418 (2.97)	0.2057	HOMO→LUMO (97%)	^{1}LLCT/^{1}MC	433
S_2	374 (3.31)	0.6701	HOMO-2→LUMO (92%)	^{1}MLCT/^{1}MC/^{1}IL	392
S_6	316 (3.92)	0.0961	HOMO→LUMO+2 (76%) HOMO→LUMO+1 (11%)	^{1}LLCT/^{1}MC ^{1}LLCT/^{1}MC/^{1}IL	
S_{10}	301 (4.12)	0.1992	HOMO→LUMO+4 (57%) HOMO→LUMO+5 (29%)	^{1}LLCT/^{1}MC/^{1}LMCT ^{1}LLCT/^{1}MC	
S_{19}	286 (4.34)	0.1870	HOMO→LUMO+10 (23%) HOMO→LUMO+7 (20%) HOMO→LUMO+9 (11%) HOMO-1→LUMO+2 (10%)	^{1}LLCT/^{1}MC/^{1}LMCT ^{1}LLCT/^{1}MC/^{1}IL ^{1}LLCT/^{1}MC/^{1}LMCT ^{1}LLCT/^{1}MC/^{1}LMCT	

Table S3. The Partial Molecular Orbital Compositions (%) by SCPA Approach in the Lowest-Energy Triplet State and the Emission Transitions for Complex **1** in the CH_2Cl_2 Solution Calculated by TD-DFT Method at the PBE1PBE Level.

orbital	energy (eV)	MO contribution (%)				
		Pt (s/p/d)	Au (s/p/d)	dTolmp	$[C{\equiv}CC_6H_4Bu^t\text{-}4]^-$	$[C{\equiv}CC_6H_4C{\equiv}CH]^-$
LUMO+1	-1.76	11.90 (59/15/26)	17.34 (55/41/3)	46.22	0.95	23.59
LUMO	-2.70	11.91 (8/90/2)	16.45 (49/33/18)	54.05	4.93	12.65
HOMO	-6.02	19.60 (10/1/90)	2.55 (46/14/39)	2.99	18.72	56.14

state	*E*, nm (eV)	O.S.	transition (contrib.)	assignment	measured (nm)
T_1	522 (2.38)	0.0000	HOMO→LUMO (61%) HOMO→LUMO+1 (17%)	^{3}LLCT/^{3}MC/^{3}LMCT ^{3}LLCT/^{3}IL/^{3}MC	507

Table S4. The Partial Molecular Orbital Compositions (%) by SCPA Approach in the Ground State and the Absorption Transitions for Complex **2** in the CH_2Cl_2 Solution Calculated by TD-DFT Method at the PBE1PBE Level.

orbital	energy (eV)	MO contribution (%)				
		Pt (s/p/d)	Au (s/p/d)	dTolmp	$[C{\equiv}CC_6H_4Bu^t\text{-}4]^-$	$[C{\equiv}CC_6H_4\text{-}C{\equiv}C]^{2-}$
LUMO+6	-1.75	13.09 (67/17/16)	13.65 (65/21/14)	70.30	2.34	0.63
LUMO+5	-1.77	17.58 (41/49/10)	10.38 (70/22/8)	69.72	0.69	1.64
LUMO+4	-1.79	22.46 (40/56/4)	11.06 (57/36/7)	53.44	0.56	1.15
LUMO+3	-1.85	27.37 (79/8/13)	10.08 (64/33/3)	59.07	1.01	2.47
LUMO+2	-1.88	7.90 (66/12/22)	10.86 (46/48/6)	77.43	1.31	2.50
LUMO+1	-2.66	13.84 (16/62/21)	18.18 (49/39/11)	61.67	3.58	2.72
LUMO	-2.75	13.15 (12/65/23)	17.30 (49/39/12)	59.11	3.48	6.96
HOMO	-6.35	22.90 (13/3/83)	2.49 (39/22/39)	4.03	26.84	43.74
HOMO-1	-6.48	18.96 (12/3/85)	6.00 (52/12/36)	6.94	45.72	22.38
HOMO-3	-6.86	32.22 (21/1/77)	39.10 (39/8/53)	25.71	0.92	2.05
HOMO-4	-6.98	34.92 (21/1/78)	38.04 (42/7/51)	25.55	0.83	0.65

state	*E*, nm (eV)	O.S.	transition (Contrib.)	assignment	measured (nm)
S_1	425 (2.92)	0.3973	HOMO→LUMO (78%)	^{1}LLCT/^{1}MC	446
			HOMO-1→LUMO+1 (10%)	^{1}LLCT/^{1}MC	
S_5	374 (3.31)	0.4211	HOMO-3→LUMO+1 (55%)	^{1}MC/^{1}MLCT/^{1}IL	390
			HOMO-3→LUMO (41%)	^{1}MC/^{1}MLCT/^{1}IL	
S_6	363 (3.42)	0.5561	HOMO-4→LUMO (69%)	^{1}MC/^{1}MLCT/^{1}IL	
			HOMO-4→LUMO+1 (28%)	^{1}MC/^{1}MLCT/^{1}IL	
S_{15}	313 (3.96)	0.2136	HOMO→LUMO+4 (27%)	^{1}LLCT/^{1}LMCT/^{1}MC	
			HOMO→LUMO+2 (13%)	^{1}LLCT/^{1}MC	
			HOMO→LUMO+5 (10%)	^{1}LLCT/^{1}MC	
S_{17}	310 (3.99)	0.2036	HOMO→LUMO+5 (29%)	^{1}LLCT/^{1}MC	
			HOMO→LUMO+4 (18%)	^{1}LLCT/^{1}LMCT/^{1}MC	
			HOMO→LUMO+6 (12%)	^{1}LLCT/^{1}MC/^{1}LMCT	

Table S5. The Partial Molecular Orbital Compositions (%) by SCPA Approach in the Lowest-Energy Triplet State and the Emission Transitions for Complex **2** in the CH_2Cl_2 Solution Calculated by TD-DFT Method at the PBE1PBE Level.

orbital	energy (eV)	MO contribution (%)				
		Pt (s/p/d)	Au (s/p/d)	dTolmp	$[C{\equiv}CC_6H_4Bu^t\text{-}4]^-$	$[C{\equiv}CC_6H_4\text{-}C{\equiv}C]^{2-}$
LUMO+2	-1.95	20.58 (77/8/15)	15.65 (69/26/5)	48.18	0.54	17.06
LUMO	-2.90	14.19 (12/61/27)	16.82 (51/35/14)	53.27	3.39	12.33
HOMO	-6.06	20.37 (13/5/82)	3.45 (39/24/37)	5.55	8.17	62.45

state	*E*, nm (eV)	O.S.	transition (contrib.)	assignment	measured (nm)
T_1	542 (2.29)	0.0000	HOMO→LUMO (62%)	^{3}LLCT/^{3}MC/^{3}IL^3	543
			HOMO→LUMO+2 (19%)	LLCT/^{3}IL/^{3}MC	

Table S6. The Partial Molecular Orbital Compositions (%) by SCPA Approach in the Ground State and the Absorption Transitions for Complex **3** in the CH_2Cl_2 Solution Calculated by TD-DFT Method at the PBE1PBE Level.

orbital	energy (eV)	MO contribution (%)				
		Pt (s/p/d)	Au (s/p/d)	dTolmp	$[C{\equiv}CC_6H_4Bu^t\text{-}4]^-$	$[C{\equiv}CCarb\text{-}C{\equiv}CH]^-$
LUMO+2	-1.66	24.89 (76/6/18)	6.45 (61/34/5)	62.80	0.92	4.94
LUMO+1	-1.71	8.82 (68/10/21)	4.06 (53/36/11)	37.34	0.34	49.44
LUMO	-2.53	12.25 (5/86/9)	20.97 (57/34/10)	57.68	2.15	6.94
HOMO	-6.11	12.05 (1/8/91)	1.08 (29/18/53)	2.76	2.57	81.55
HOMO-3	-6.76	35.14 (22/0/77)	37.58 (41/9/51)	25.75	0.60	0.94

state	*E*, nm (eV)	O.S.	transition (contrib.)	assignment	
S_1	422 (2.93)	0.4729	HOMO→LUMO (95%)	^{1}LLCT/^{1}LMCT/^{1}MC	435
S_3	374 (3.32)	0.6383	HOMO-3→LUMO (97%)	^{1}MC/^{1}MLCT/^{1}IL	392
S_7	324 (3.83)	0.9382	HOMO→LUMO+1 (80%) HOMO→LUMO+2 (12%)	^{1}IL/^{1}LLCT/^{1}MC ^{1}LLCT/^{1}LMCT/^{1}MC	

Table S7. The Partial Molecular Orbital Compositions (%) by SCPA Approach in the Lowest-Energy Triplet State and the Emission Transitions for Complex **3** in the CH_2Cl_2 Solution Calculated by TD-DFT Method at the PBE1PBE Level.

Orbital	Energy (eV)	MO Contribution (%)				
		Pt (s/p/d)	Au (s/p/d)	dTolmp	$[C{\equiv}CC_6H_4Bu^t\text{-}4]^-$	$[C{\equiv}CCarbC{\equiv}CH]^-$
LUMO+1	-1.81	5.01 (47/12/41)	5.44 (58/33/9)	25.94	0.22	63.39
LUMO	-2.73	13.13 (6/83/10)	22.23 (61/28/11)	54.14	2.13	8.36
HOMO	-5.86	11.79 (2/14/85)	1.61 (29/20/51)	3.06	2.06	81.49
HOMO-3	-6.76	33.32 (28/1/71)	37.76 (38/11/52)	27.40	0.69	0.83

state	*E*, nm (eV)	O.S.	transition (Contrib.)	assignment	
T_1	538 (2.30)	0.0000	HOMO→LUMO (63%) HOMO→LUMO+1 (28%)	^{3}LLCT/^{3}LMCT/^{3}MC ^{3}IL/^{3}LLCT/^{3}MC	520

Table S8. The Partial Molecular Orbital Compositions (%) by SCPA Approach in the Ground State and the Absorption Transitions for Complex **4** in the CH_2Cl_2 Solution Calculated by TD-DFT Method at the PBE1PBE Level.

orbital	energy (eV)	MO contribution (%)				
		Pt (s/p/d)	Au (s/p/d)	dTolmp	$[C{\equiv}CC_6H_4Bu^t\text{-}4]^-$	$[C{\equiv}CCarb\text{-}C{\equiv}C]^{2-}$
LUMO+2	-1.87	12.70 (73/7/21)	16.87 (60/36/4)	35.72	0.38	34.25
LUMO+1	-2.55	10.41 (4/91/5)	20.67 (54/35/12)	63.07	2.54	3.31
LUMO	-2.69	11.44 (6/88/6)	20.87 (56/32/12)	53.14	2.63	11.59
HOMO	-6.25	14.94 (1/2/96)	3.56 (58/12/29)	4.50	4.86	72.13
HOMO-1	-6.58	10.24 (1/5/94)	0.57 (33/23/44)	8.06	79.03	2.10
HOMO-3	-6.73	33.94 (27/0/72)	39.45 (39/11/50)	25.24	0.87	0.51
HOMO-4	-6.76	33.96 (27/0/73)	39.40 (39/11/50)	25.59	0.45	0.60
HOMO-5	-6.81	1.36 (60/17/23)	2.72 (53/29/18)	2.84	0.04	93.04
HOMO-6	-7.01	33.99 (5/0/94)	1.81 (46/17/37)	4.10	19.07	41.04

state	*E*, nm (eV)	O.S.	transition (contrib.)	assignment	measured (nm)
S_1	425 (2.92)	0.7542	HOMO→LUMO (92%)	^{1}LLCT/^{1}MC/^{1}LMCT	449
S_5	375 (3.30)	0.4475	HOMO-3→LUMO (59%)	^{1}MC^1/MLCT/^{1}IL	393
			HOMO-3→LUMO+1 (35%)	^{1}MC/^{1}MLCT/^{1}IL	
S_6	373 (3.33)	0.8801	HOMO-4→LUMO (55%)	^{1}MC^1/MLCT/^{1}IL	
			HOMO-4→LUMO+1 (40%)	^{1}MC^1/MLCT/^{1}IL	
S_{10}	329 (3.77)	0.2995	HOMO-6→LUMO (11%)	^{1}LLCT/^{1}MC	
			HOMO-5→LUMO+1 (12%)	^{1}LLCT/^{1}LMCT	
			HOMO-1→LUMO (10%)	^{1}LLCT/^{1}LMCT	
			HOMO-1→LUMO+1 (11%)	^{1}LLCT/^{1}LMCT	
			HOMO→LUMO+2 (34%)	^{1}IL/^{1}LLCT/^{1}MC	
S_{12}	325 (3.81)	0.3483	HOMO-5→LUMO+1 (64%)	^{1}LLCT/^{1}LMCT	
			HOMO→LUMO+2 (26%)	^{1}IL/^{1}LLCT/^{1}MC	

Table S9. The Partial Molecular Orbital Compositions (%) by SCPA Approach in the Lowest-Energy Triplet States and the Emission Transitions for Complex **4** in the CH_2Cl_2 Solution Calculated by TD-DFT Method at the PBE1PBE Level.

orbital	energy (eV)	MO contribution (%)				
		Pt (s/p/d)	Au (s/p/d)	dTolmp	$[C{\equiv}CC_6H_4Bu^t\text{-}4]^-$	$[C{\equiv}CCarb\text{-}C{\equiv}C]^{2-}$
LUMO+2	-2.03	15.87 (76/11/14)	18.41 (66/30/4)	35.92	0.51	29.30
LUMO	-2.84	12.31 (3/4/93)	21.34 (61/13/26)	45.29	2.52	18.54
HOMO	-5.96	13.06 (76/11/14)	4.86 (66/30/4)	5.02	3.27	73.79

state	*E*, nm (eV)	O.S.	transition (contrib.)	assignment	measured (nm)
T_1	548 (2.26)	0.0000	HOMO→LUMO (68%)	^{3}LLCT/^{3}MC/^{3}LMCT	544
			HOMO→LUMO+2 (23%)	^{3}LLCT/^{3}MC/^{3}LMCT	

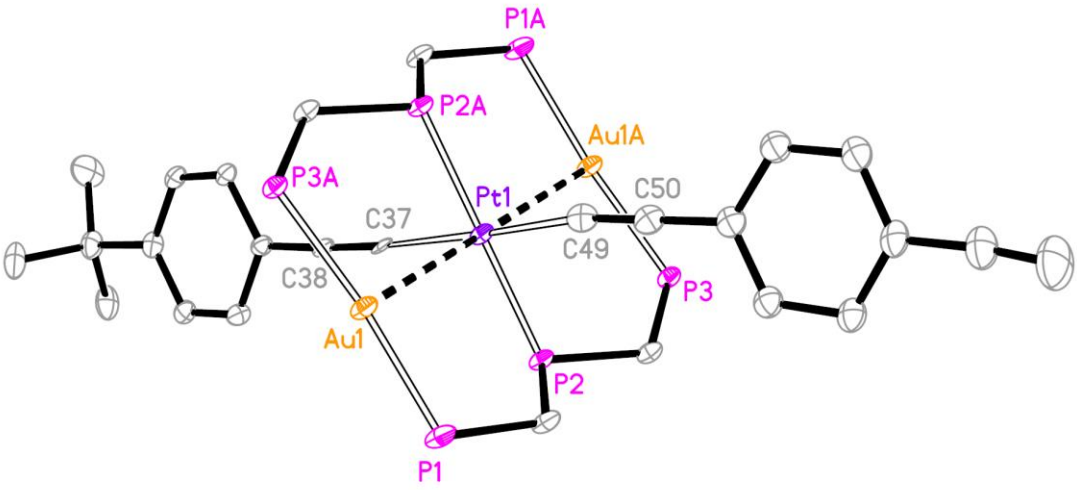

Figure S1. A perspective view of $PtAu_2$ complex **1** from X-ray crystallography showing 30% thermal ellipsoids. The phenyl and 2-methylphenyl groups in triphosphine ligands and the hydrogen atoms together with trifluoromethanesulfonates were omitted for clarity.

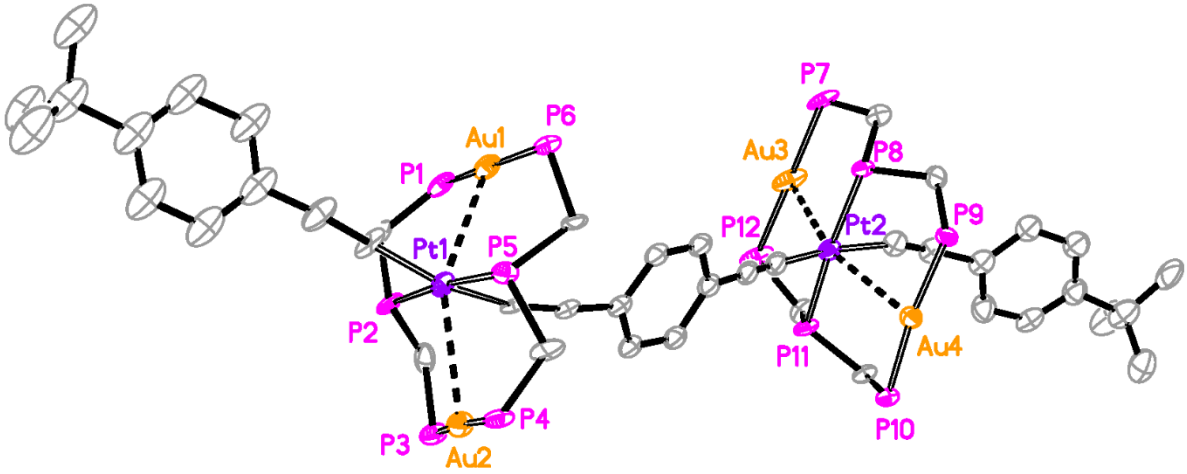

Figure S2. A perspective view of Pt_2Au_4 complex **2** from X-ray crystallography showing 30% thermal ellipsoids. The phenyl and 2-methylphenyl groups in triphosphine ligands and the hydrogen atoms together with trifluoromethanesulfonates were omitted for clarity.

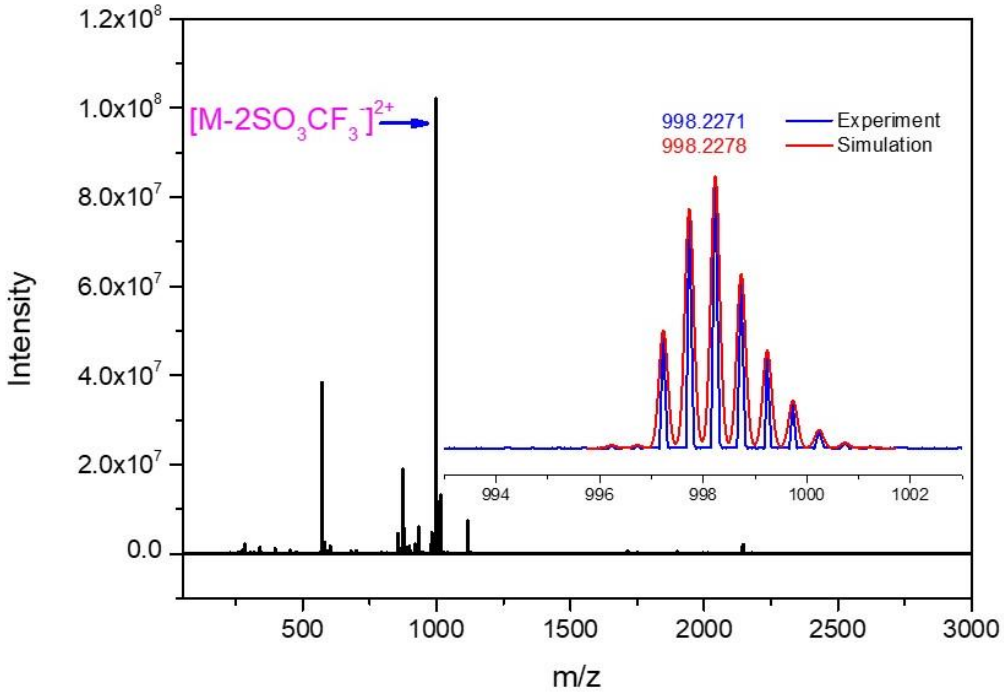

Figure S3. The high-resolution mass spectrometry of complex **1**. Inset: The measured and simulated isotopic patterns.

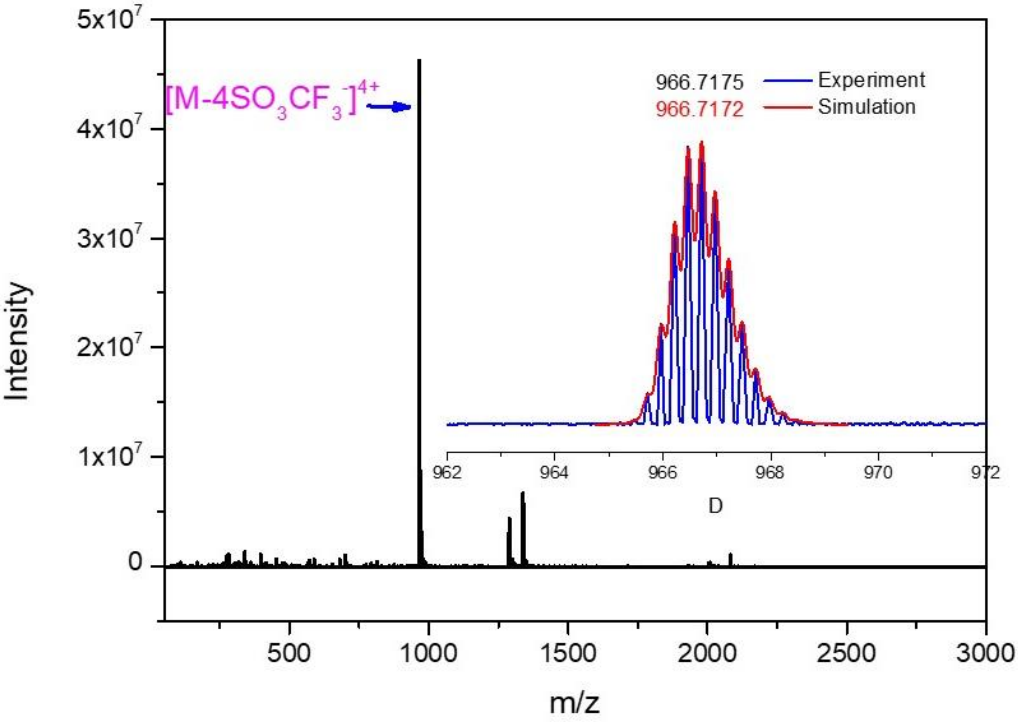

Figure S4. The high-resolution mass spectrometry of complex **2**. Inset: The measured and simulated isotopic patterns.

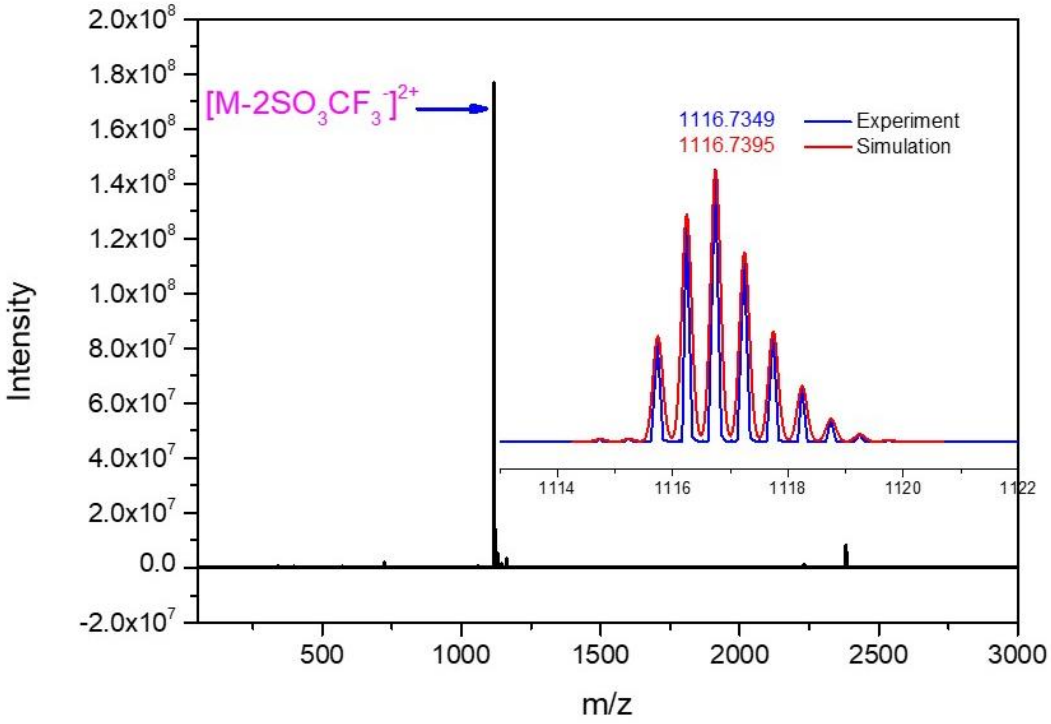

Figure S5. The high-resolution mass spectrometry of complex **3**. Inset: The measured and simulated isotopic patterns.

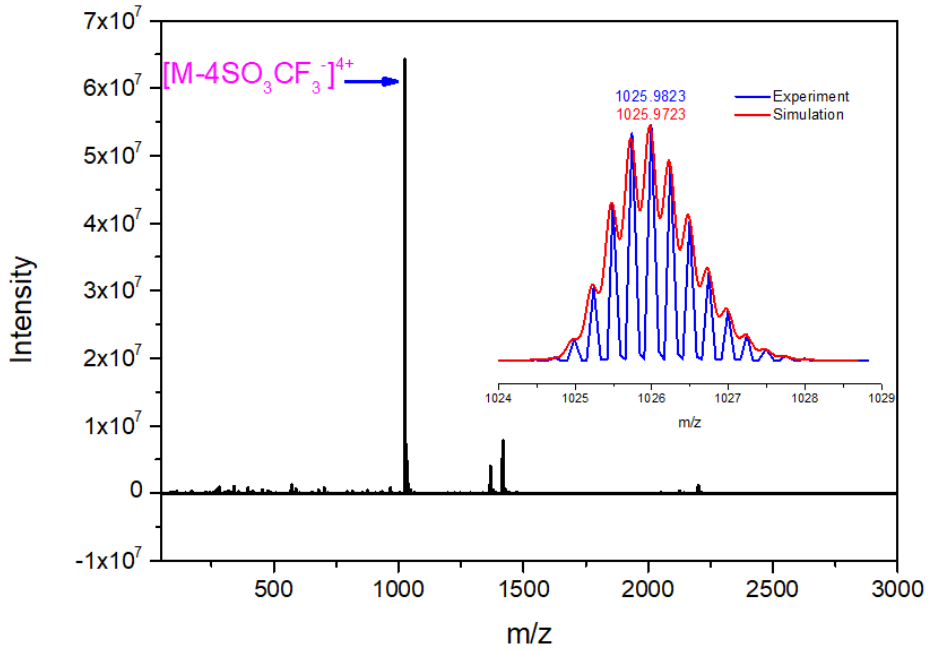

Figure S6. The high-resolution mass spectrometry of complex **4**. Inset: The measured and simulated isotopic patterns.

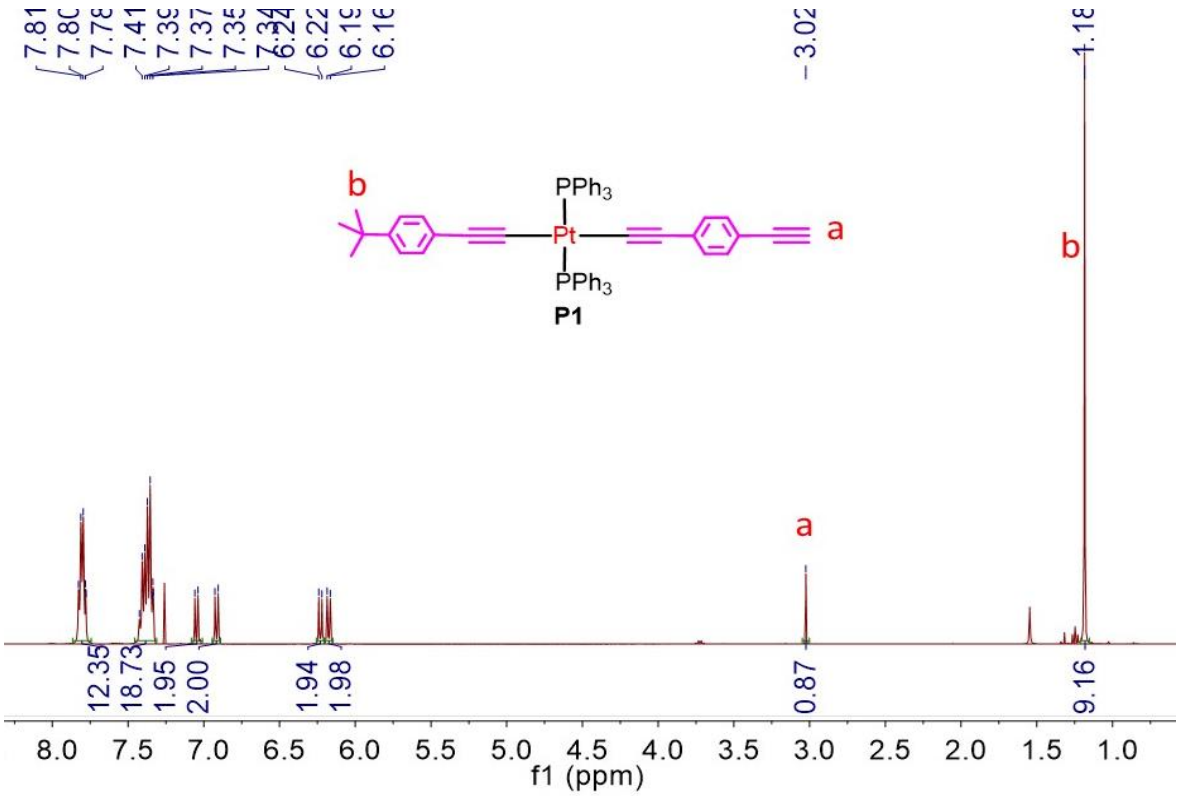

Figure S7. The ^{1}H NMR spectrum of complex **P1** in $CDCl_3$ at ambient temperature.

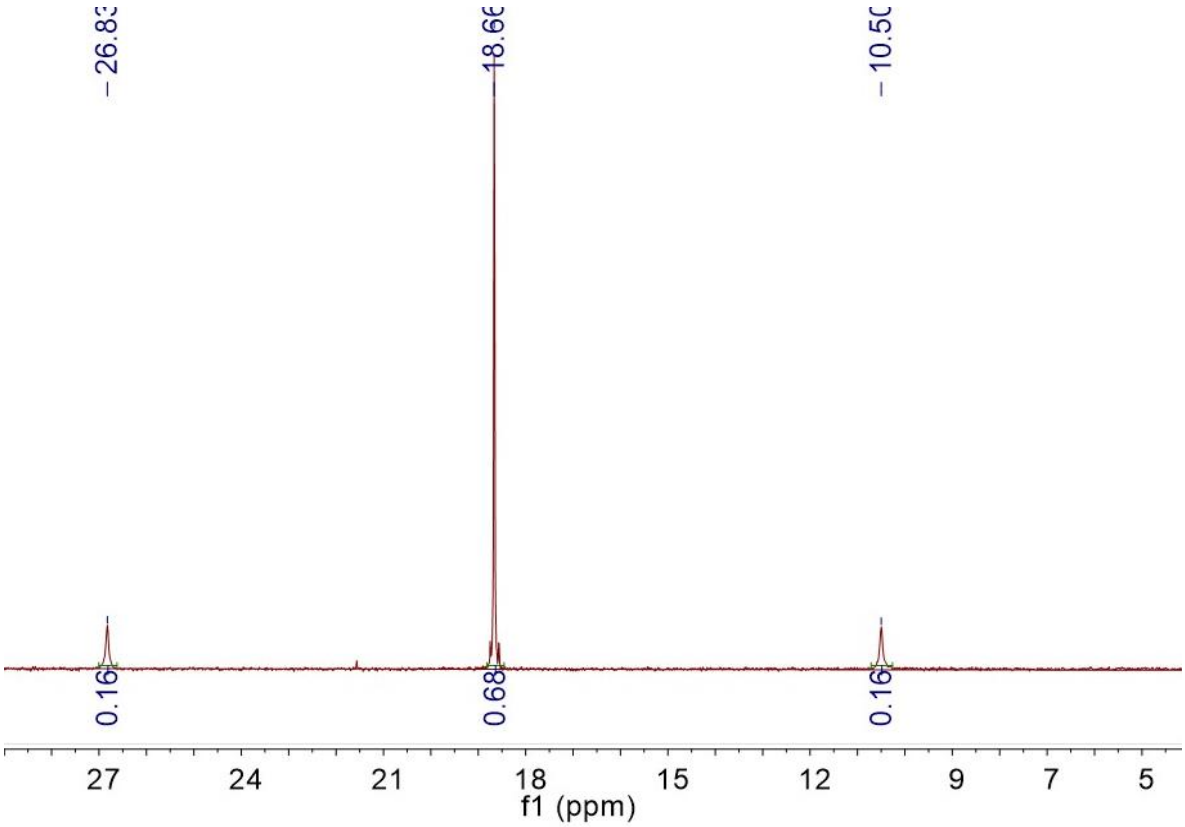

Figure S8. The ^{31}P NMR spectrum of complex **P1** in $CDCl_3$ at ambient temperature.

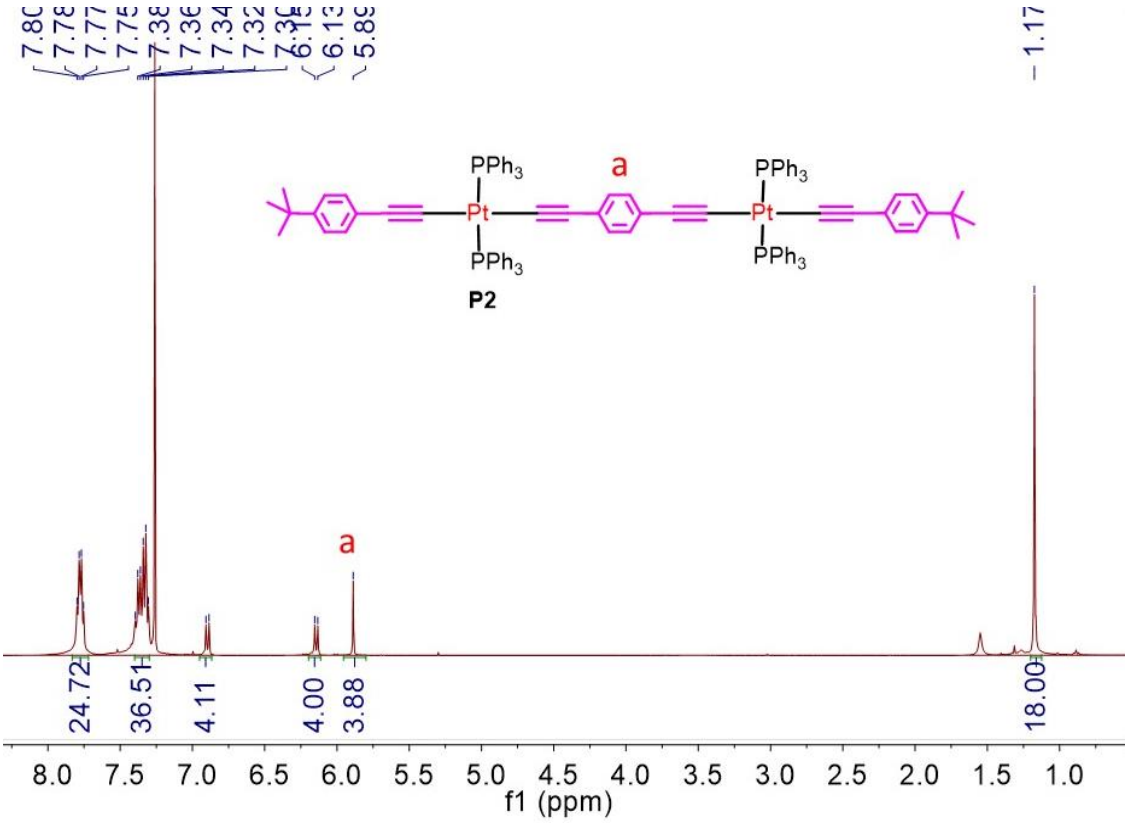

Figure S9. The ^{1}H NMR spectrum of complex **P2** in $CDCl_3$ at ambient temperature.

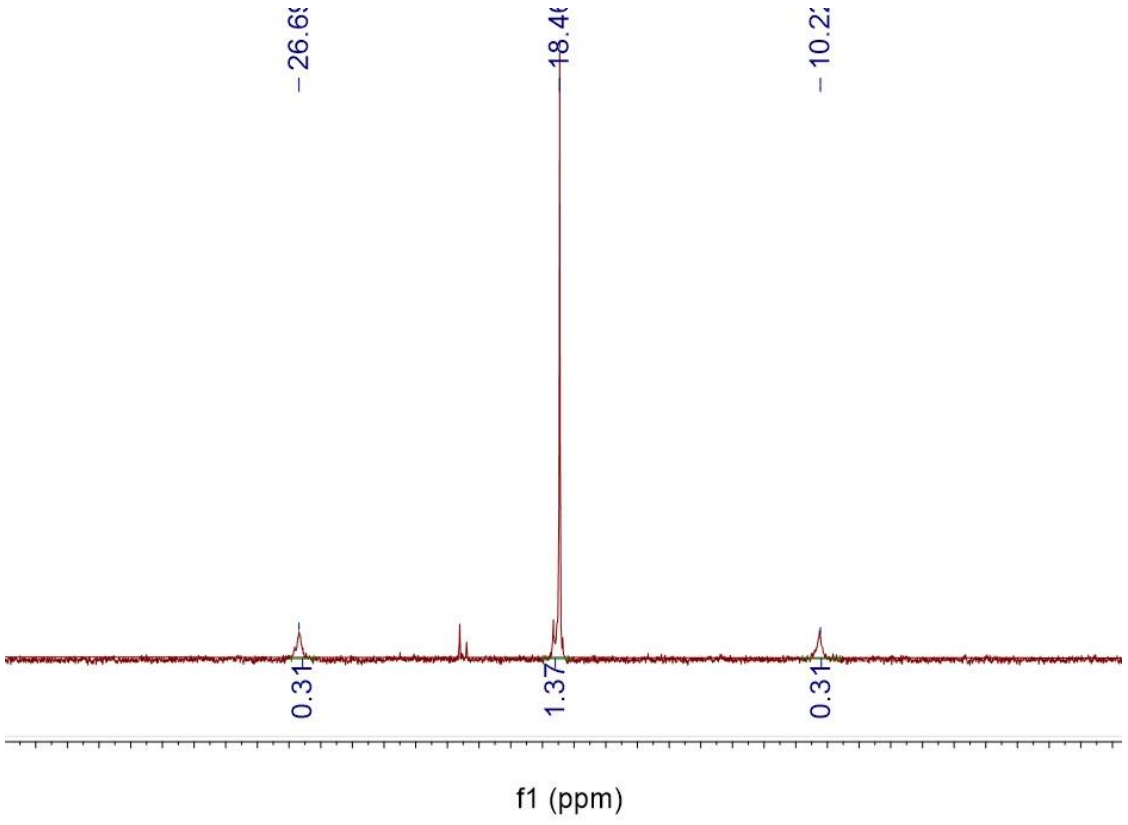

Figure S10. The ^{31}P NMR spectrum of complex **P2** in $CDCl_3$ at ambient temperature.

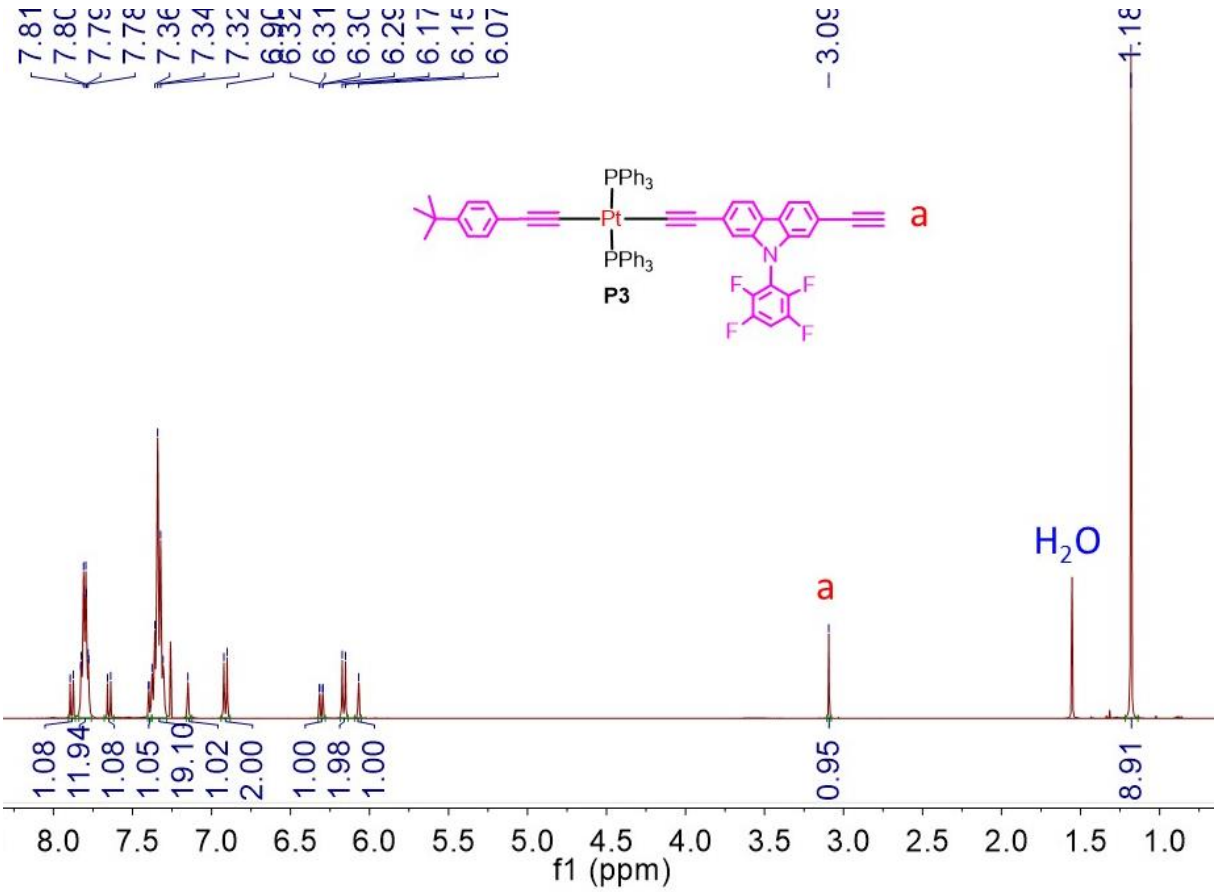

Figure S11. The ^{1}H NMR spectrum of complex **P3** in $CDCl_3$ at ambient temperature.

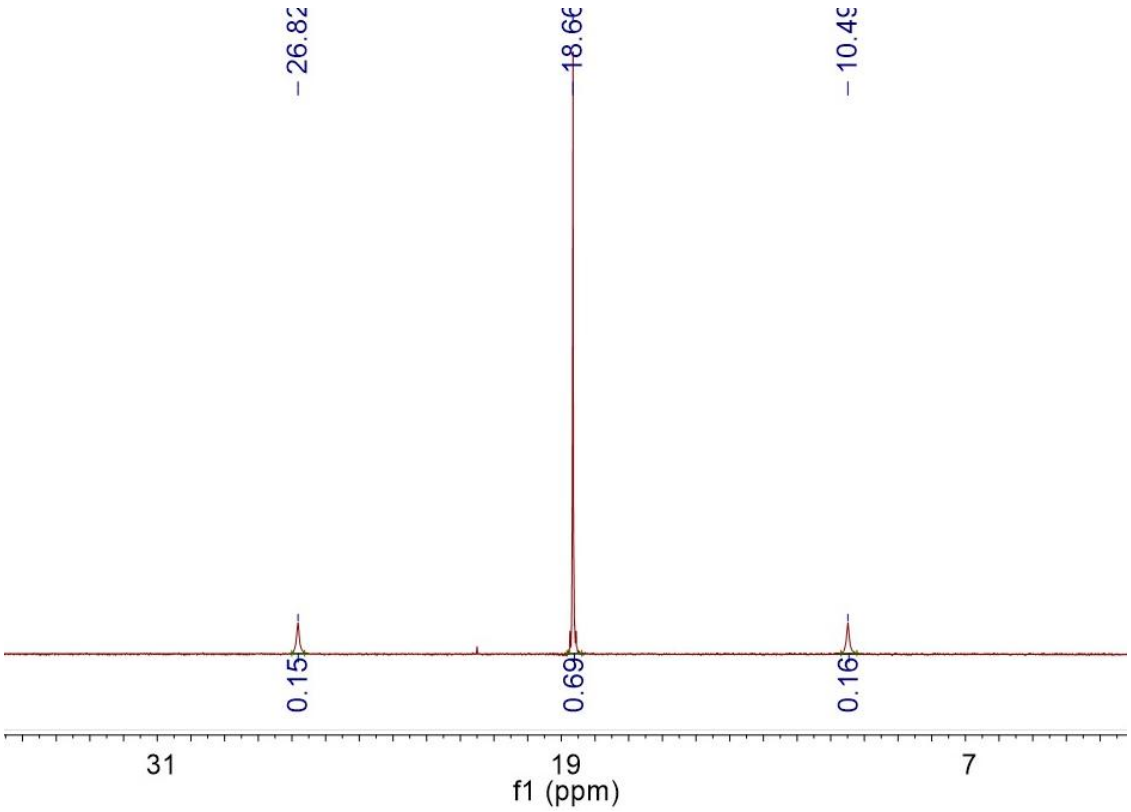

Figure S12. The ^{31}P NMR spectrum of complex **P3** in $CDCl_3$ at ambient temperature.

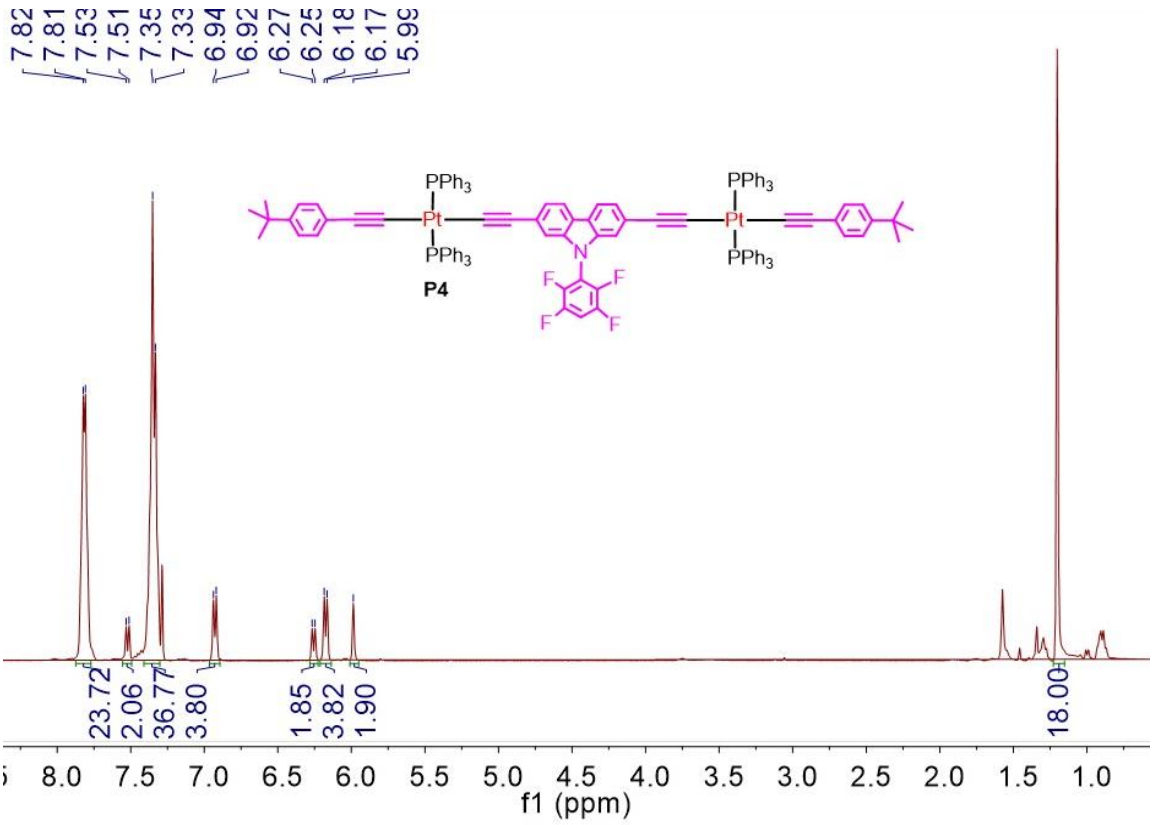

Figure S13. The ^{1}H NMR spectrum of complex **P4** in $CDCl_3$ at ambient temperature.

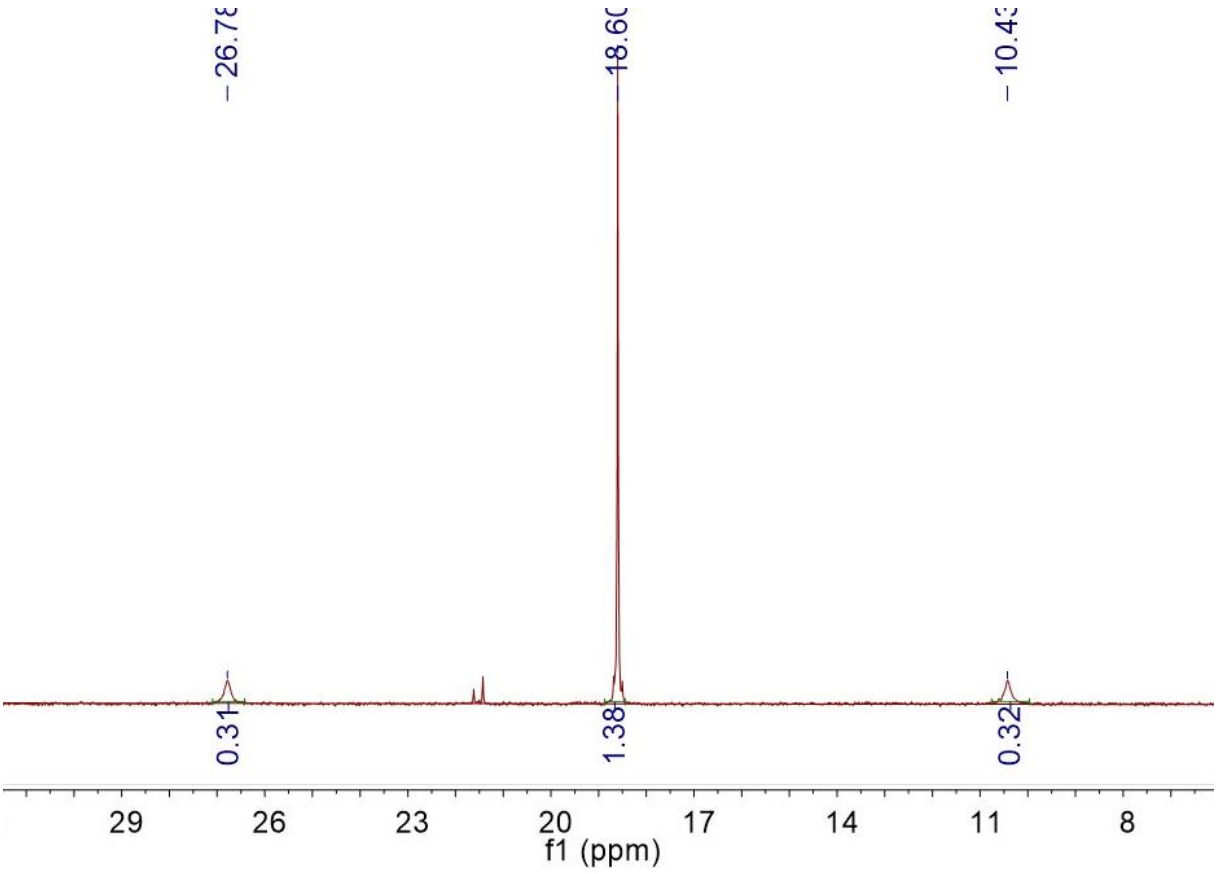

Figure S14. The ^{31}P NMR spectrum of complex **P4** in $CDCl_3$ at ambient temperature.

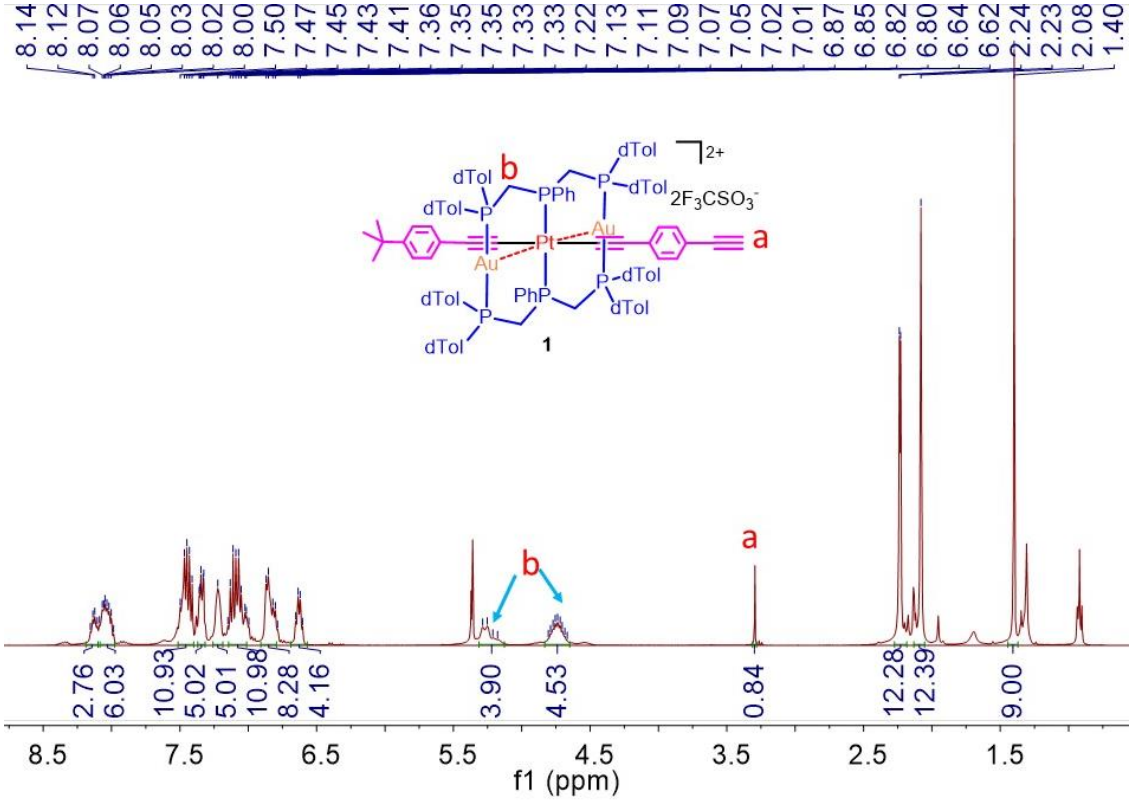

Figure S15. The ^{1}H NMR spectrum of complex **1** in CD_2Cl_2 at ambient temperature.

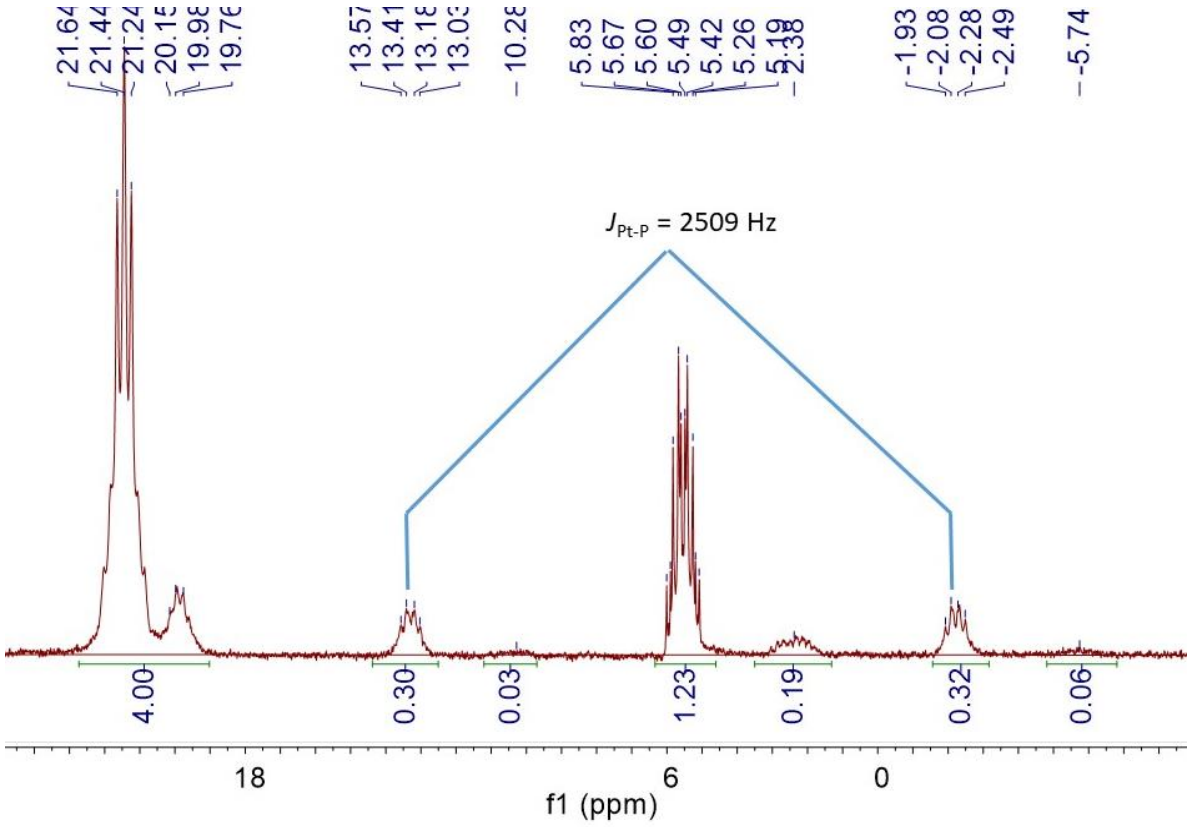

Figure S16. The ^{31}P NMR spectrum of complex **1** in CD_2Cl_2 at ambient temperature.

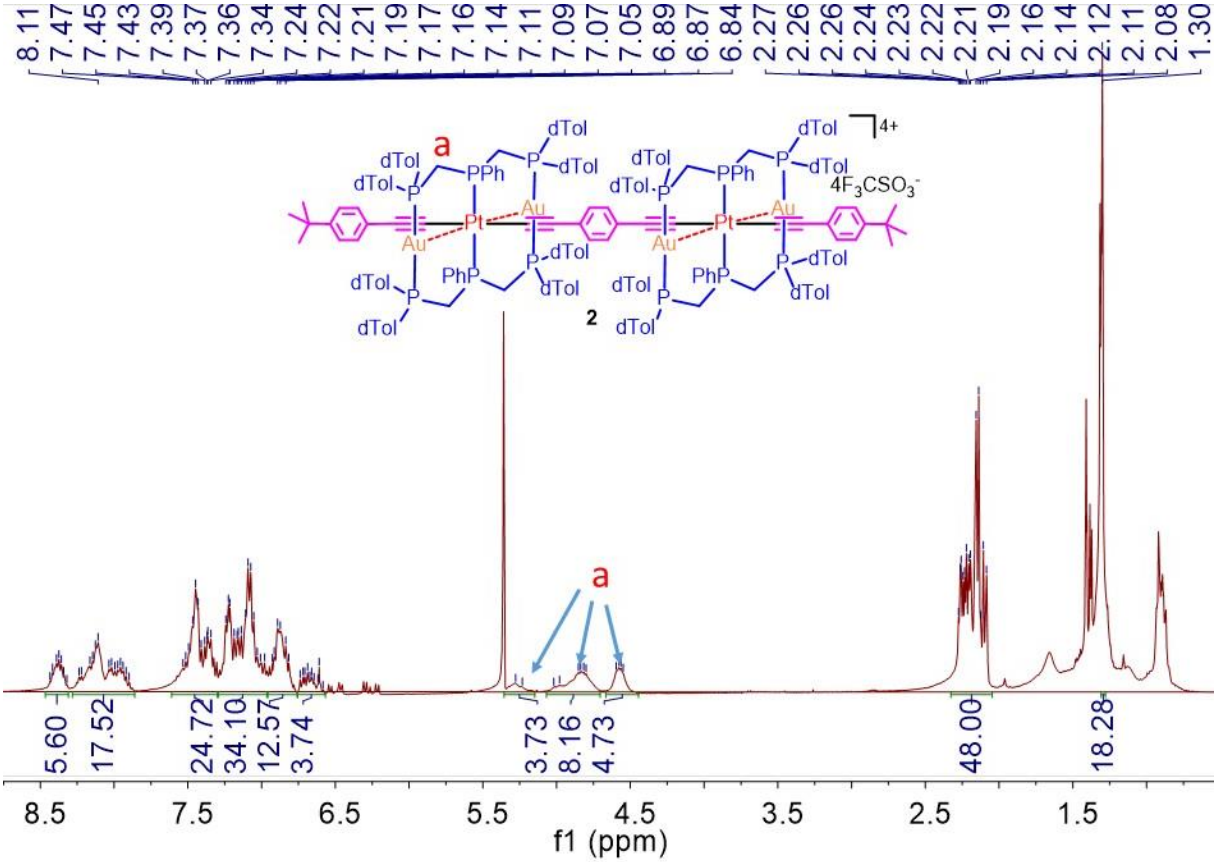

Figure S17. The ^{1}H NMR spectrum of complex **2** in CD_2Cl_2 at ambient temperature.

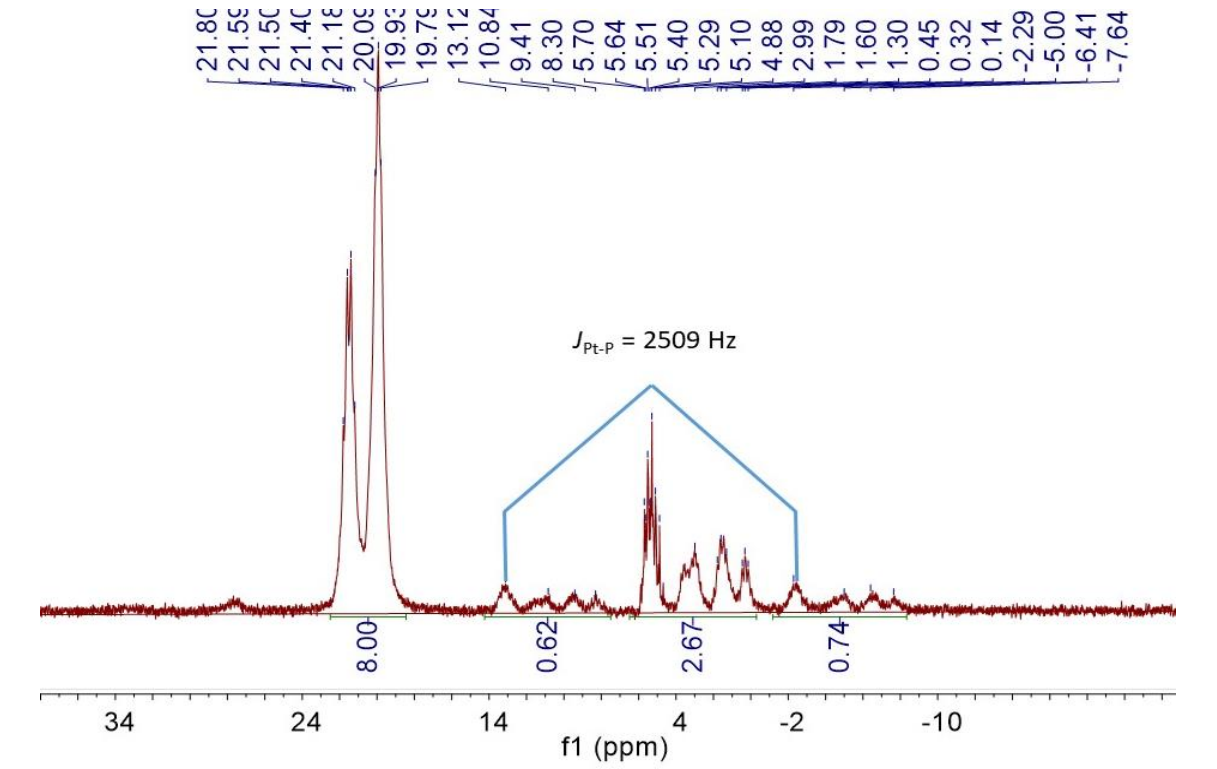

Figure S18. The ^{31}P NMR spectrum of complex **2** in CD_2Cl_2 at ambient temperature.

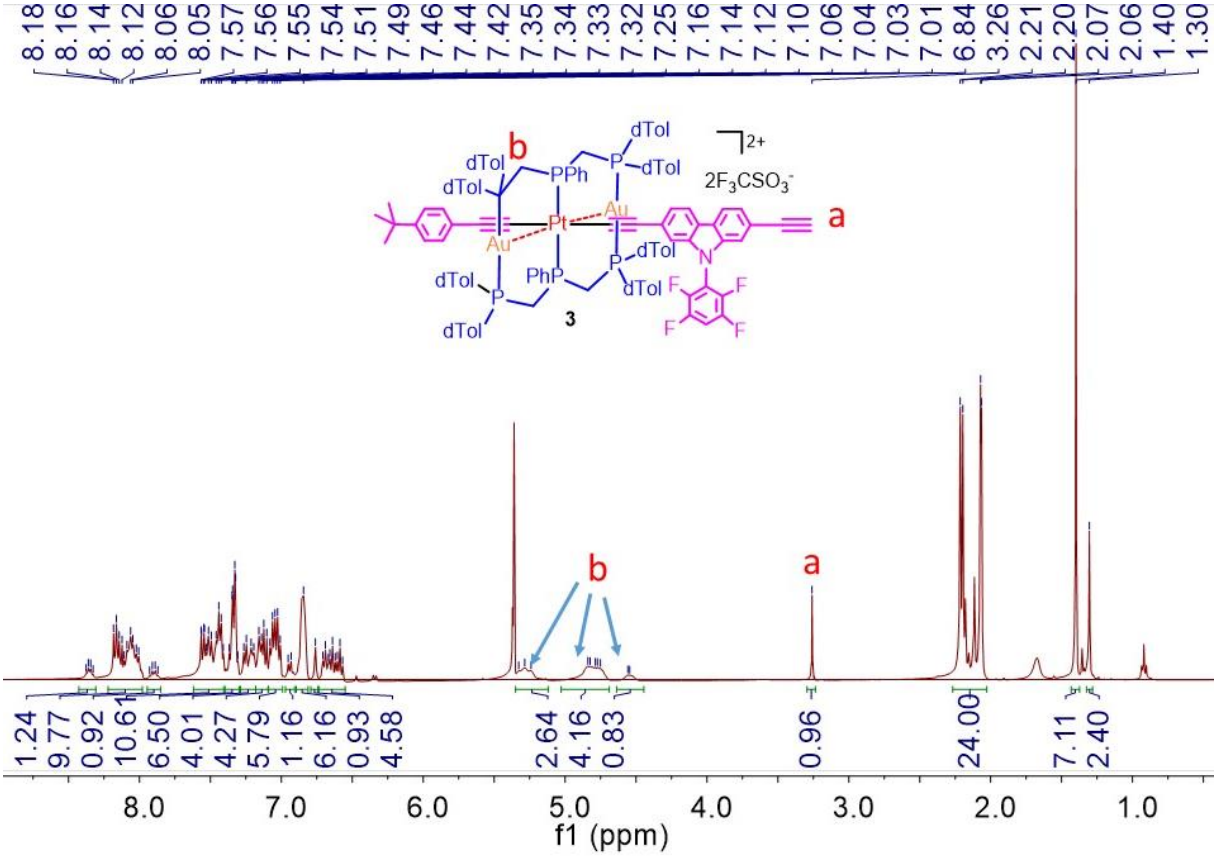

Figure S19. The ^{1}H NMR spectrum of complex **3** in CD_2Cl_2 at ambient temperature.

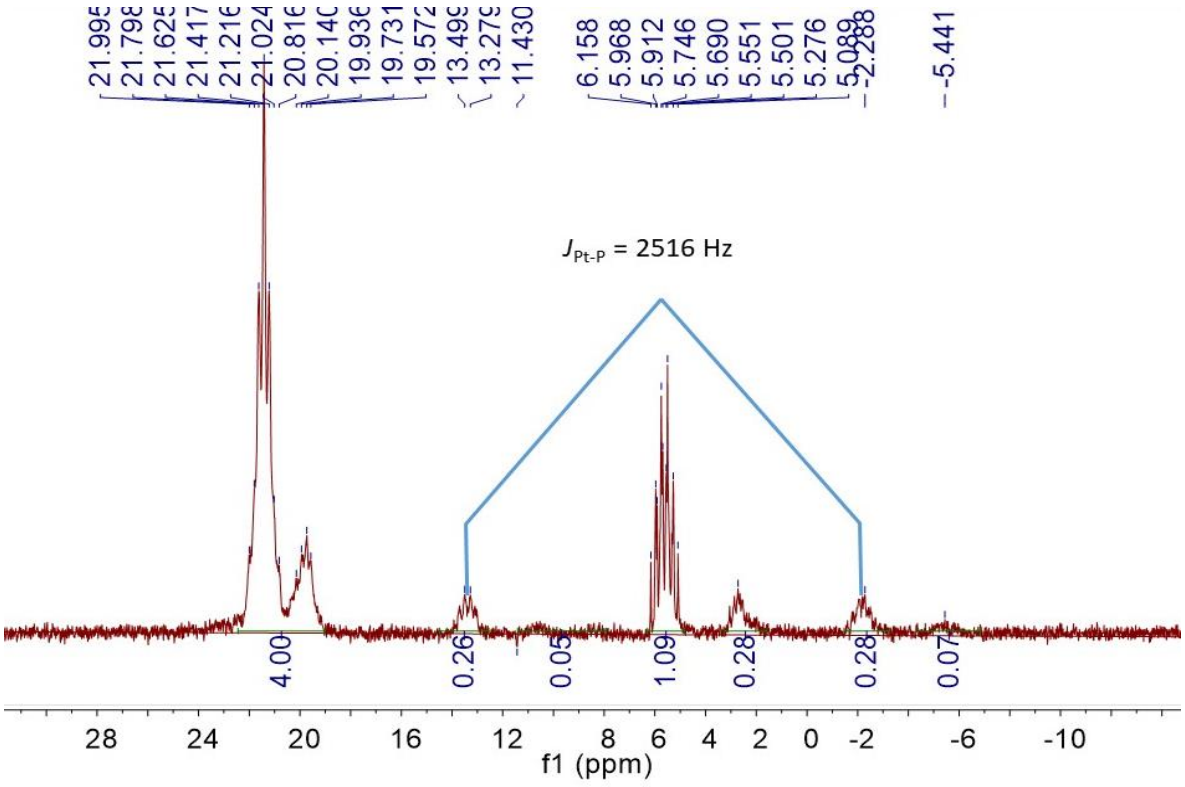

Figure S20. The ^{31}P NMR spectrum of complex **3** in CD_2Cl_2 at ambient temperature.

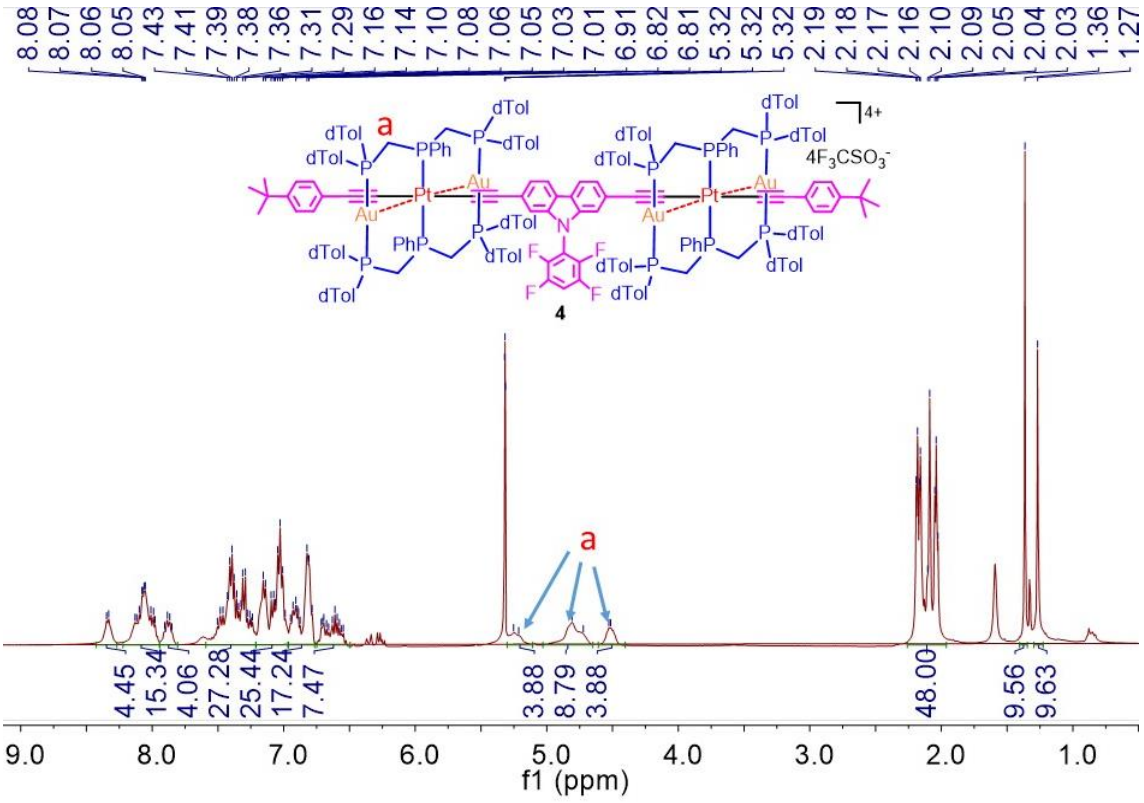

Figure S21. The ^{1}H NMR spectrum of complex **4** in CD_2Cl_2 at ambient temperature.

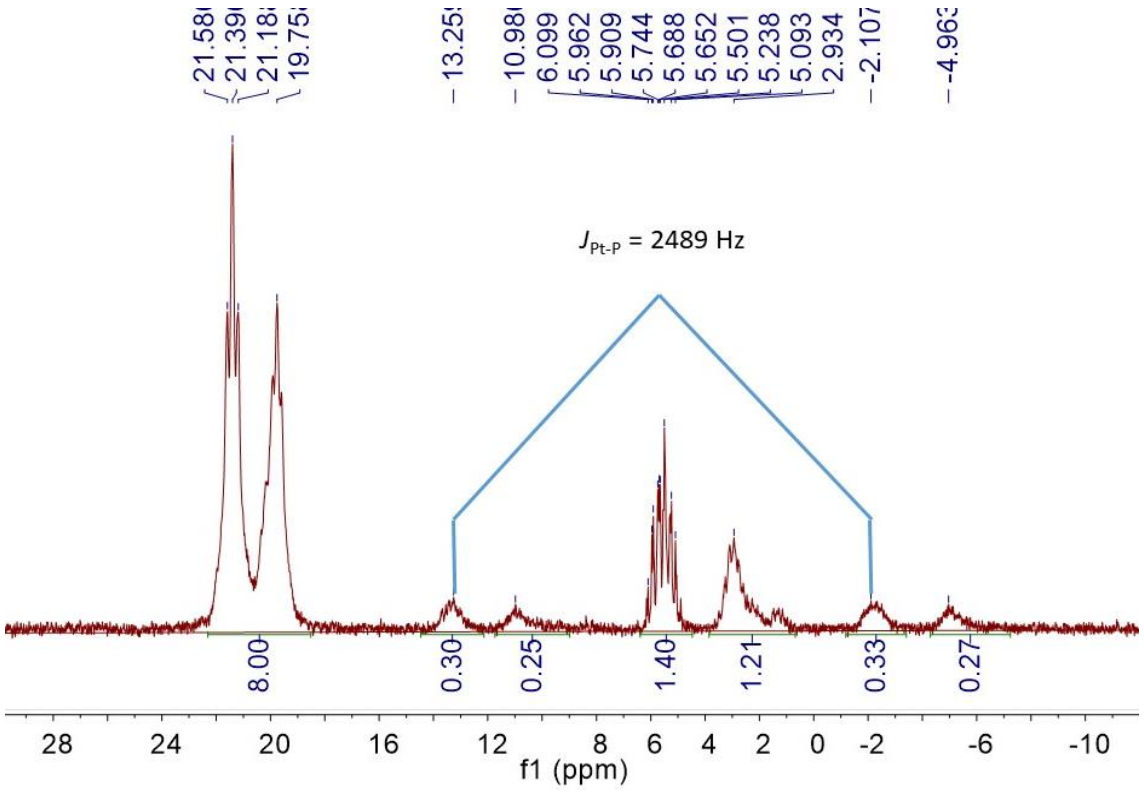

Figure S22. The ^{31}P NMR spectrum of complex **4** in CD_2Cl_2 at ambient temperature.

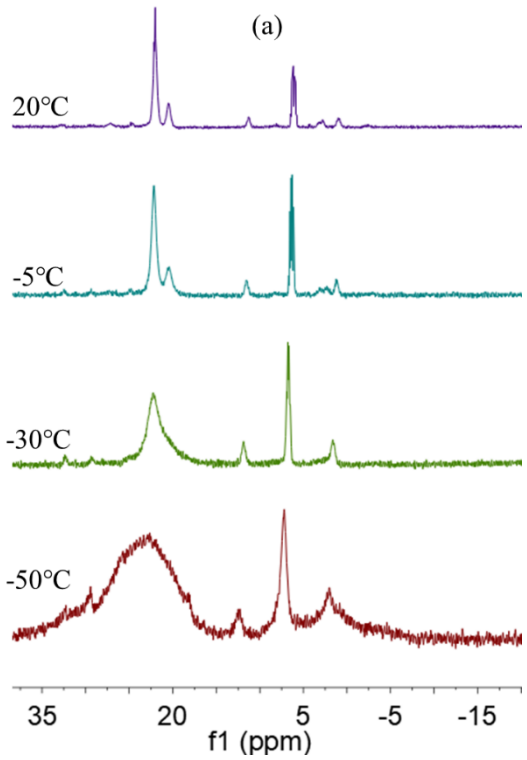

Figure S23. Varable-temperature ^{31}P NMR spectra of complex **1** in CD_2Cl_2 solution at 20, –5 , –30 and –50 ℃.

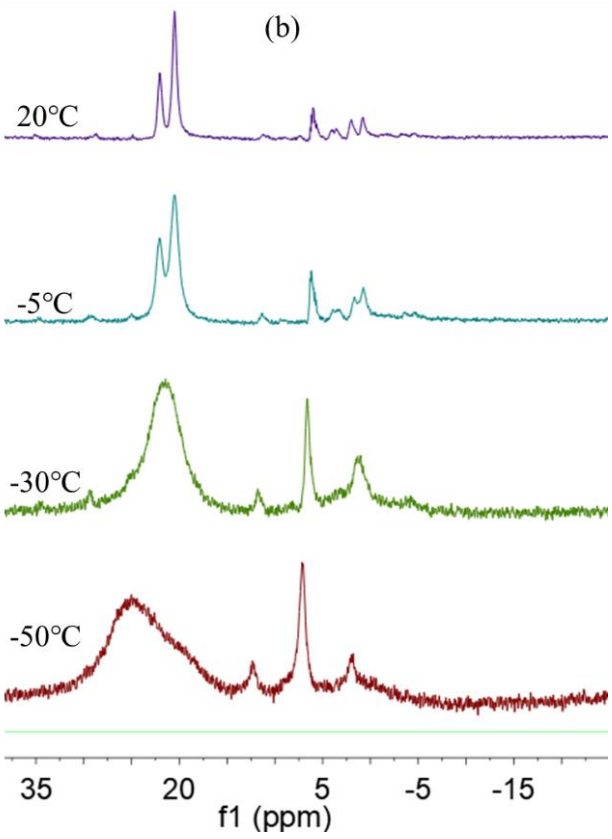

Figure S24. Varable-temperature ^{31}P NMR spectra of complex **2** in CD_2Cl_2 solution at 20, –5 , –30 and –50 ℃.

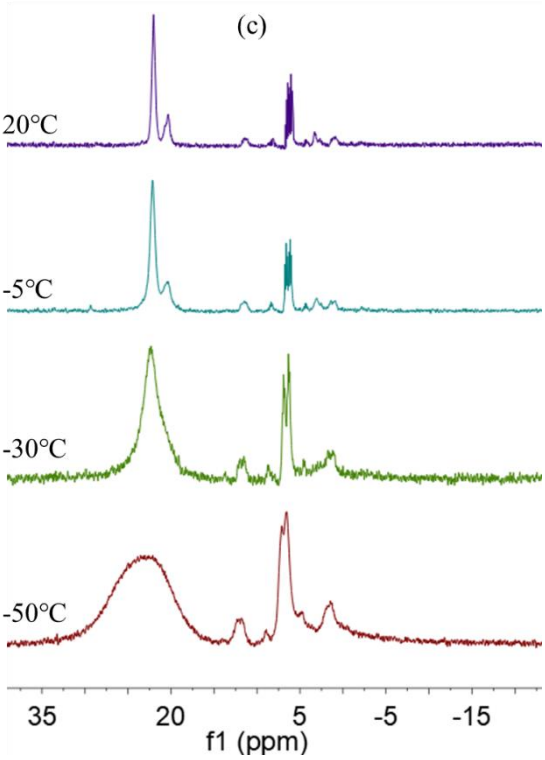

Figure S25. Varable-temperature ^{31}P NMR spectra of complex **3** in CD_2Cl_2 solution at 20, –5 , –30 and –50 ℃.

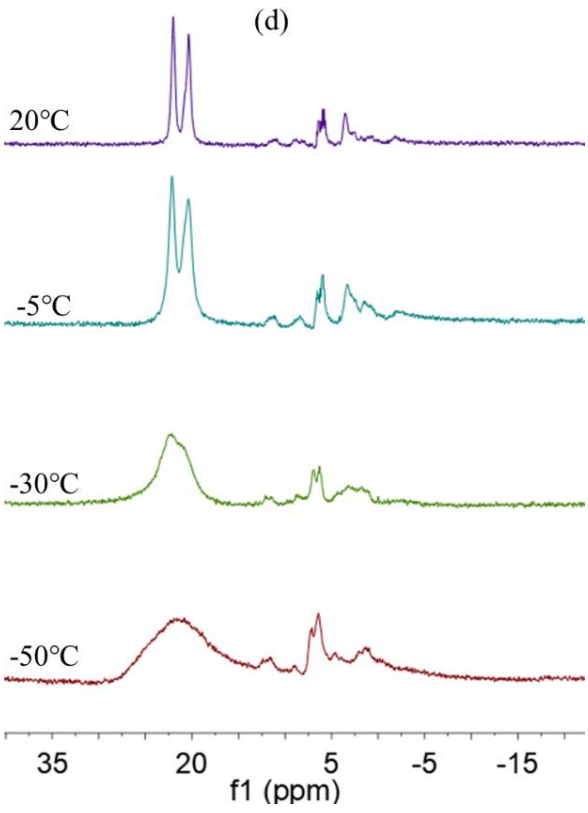

Figure S26. Varable-temperature ^{31}P NMR spectra of complex **4** in CD_2Cl_2 solution at 20, –5 , –30 and –50 ℃.

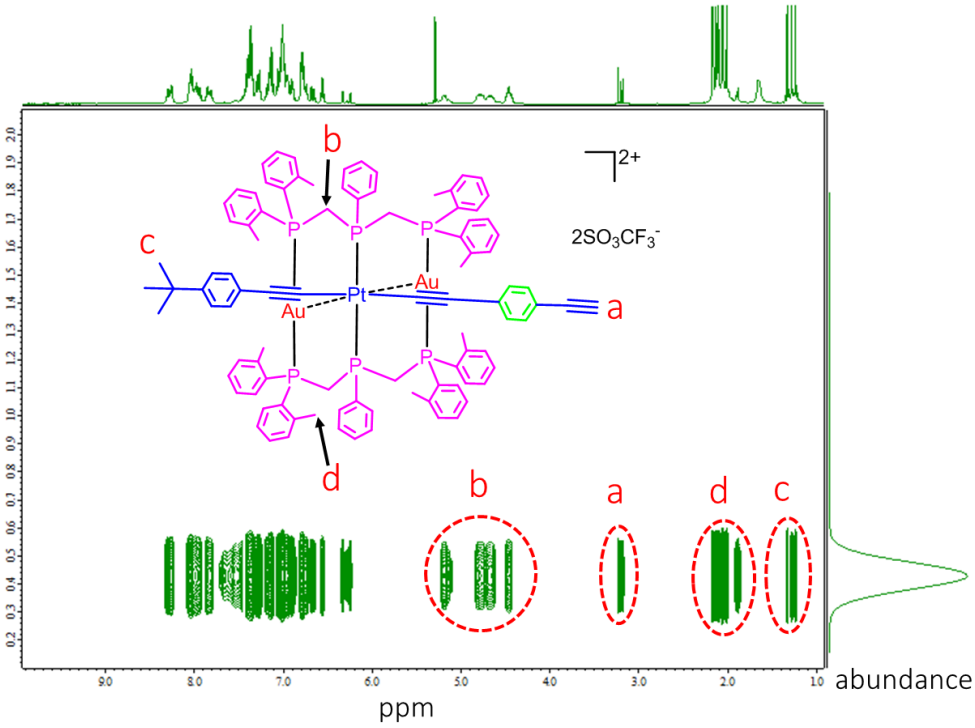

Figure S27. The DOSY NMR (400 MHz**)** spectrum of complex **1** in CD_2Cl_2 solution at 25 °C. Signals diffuse with observed diffusion coefficient value of 7.69×10^{-11} m^2/s.

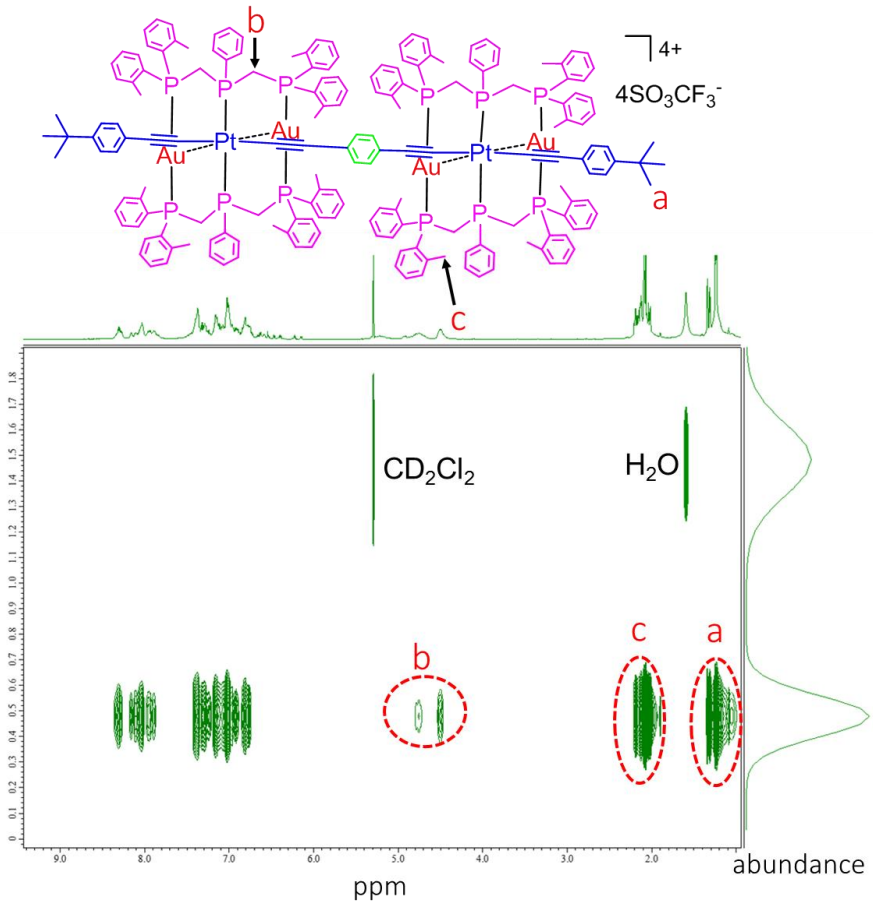

Figure S28. The DOSY NMR (400 MHz**)** spectrum of complex **2** in CD_2Cl_2 solution at 25 °C.

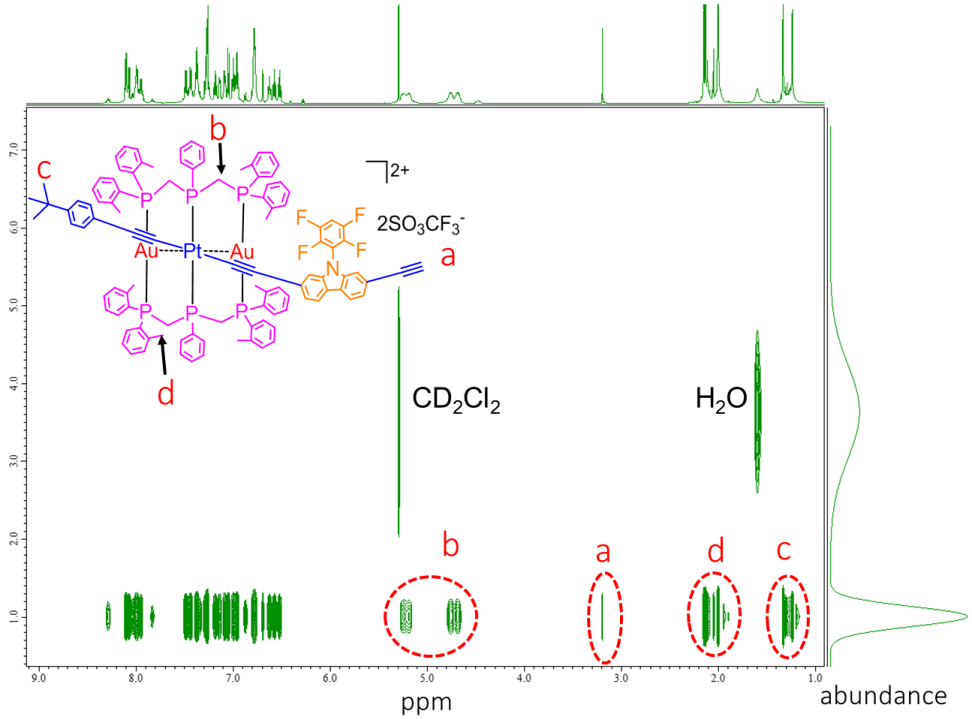

Figure S29. The DOSY NMR (400 MHz**)** spectrum of complex **3** in CD_2Cl_2 solution at 25 °C.

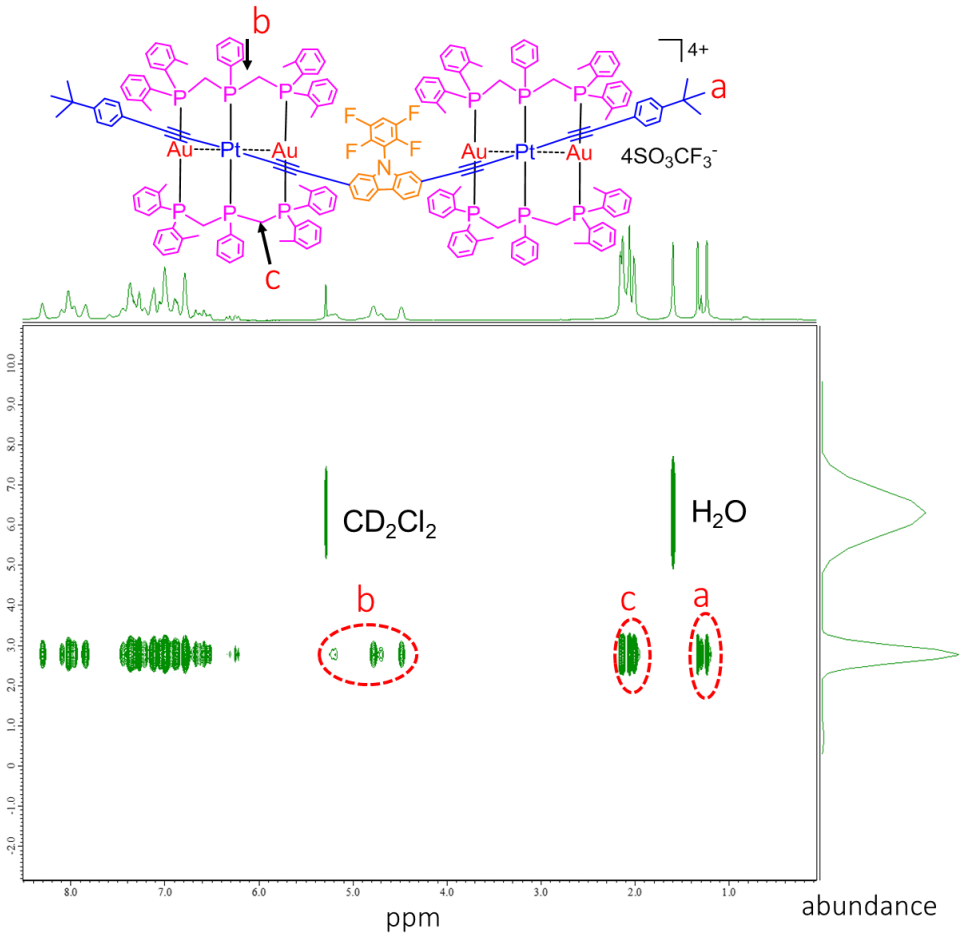

Figure S30. The DOSY NMR (400 MHz**)** spectrum of complex **4** in CD_2Cl_2 solution at 25 °C.

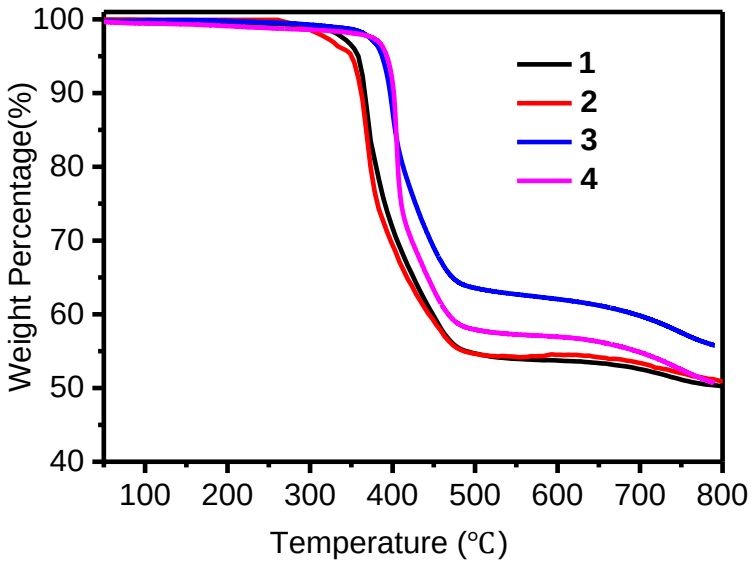

Figure S31. Plots of thermogravimetric analysis for complexes **1**–**4**.

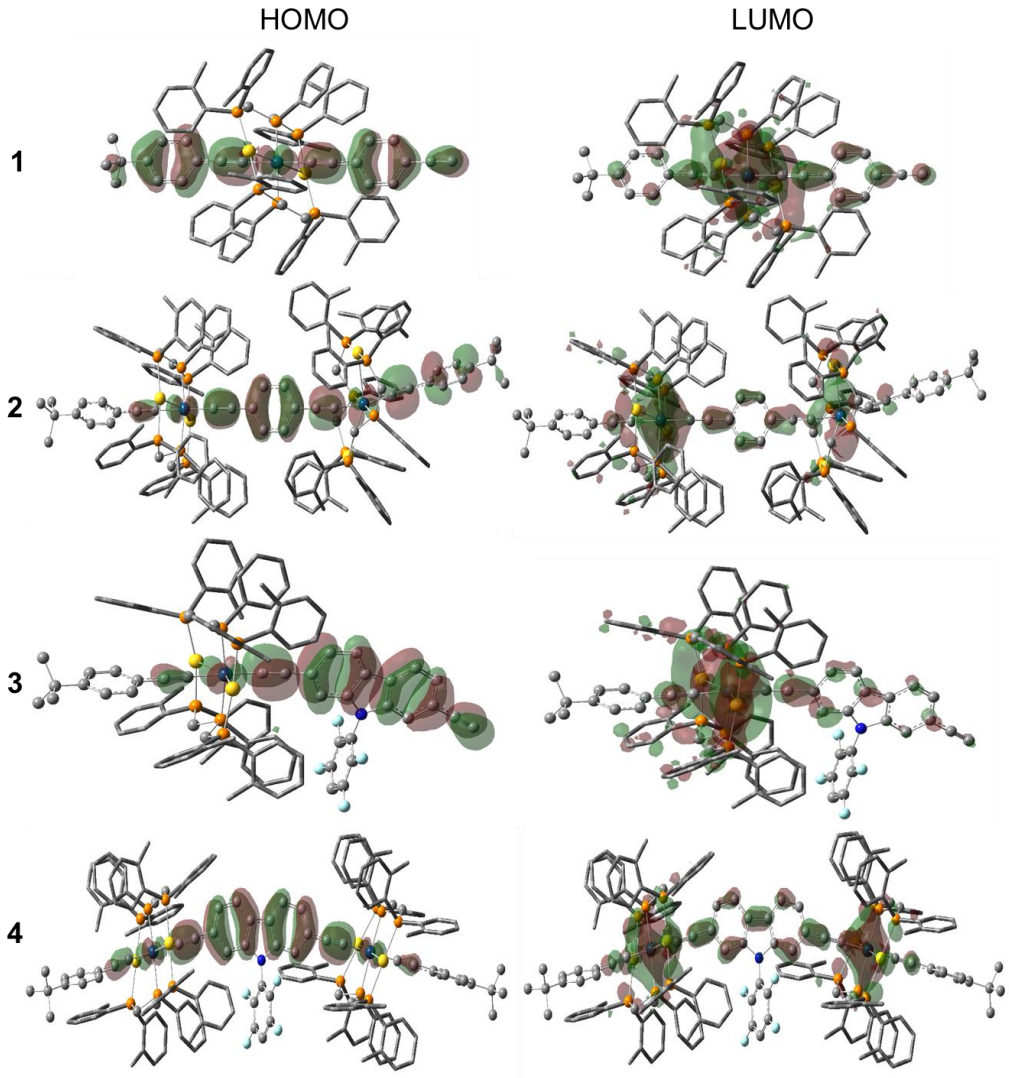

Figure S32. Plots of the HOMO and LUMO involved in the absorption transition (isovalue = 0.02) for complexes **1**–**4** by TD-DFT method at the PBE1PBE level.

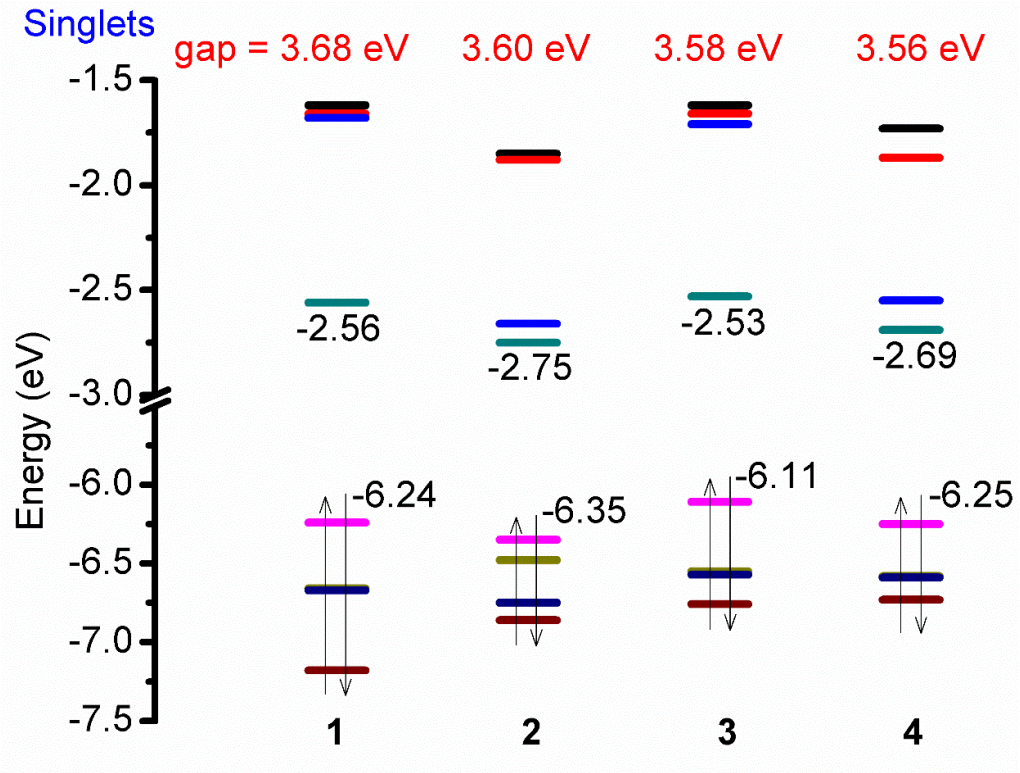

Figure S33. Plots of the energy levels of frontier molecular orbitals based on the ground state structures of complexes **1**–**4** by TD-DFT method at the PBE1PBE level.

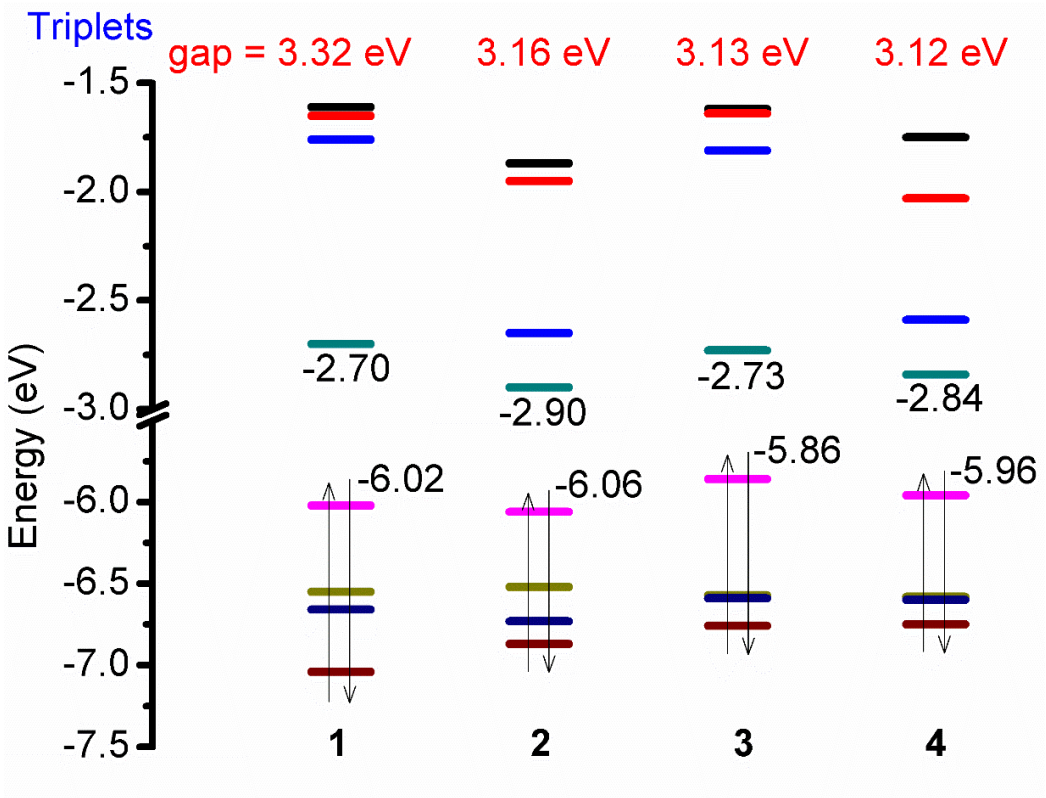

Figure S34. Plots of the energy levels of frontier molecular orbitals based on the lowest-energy triplet state structures of complexes **1**–**4** by TD-DFT method at the PBE1PBE level.

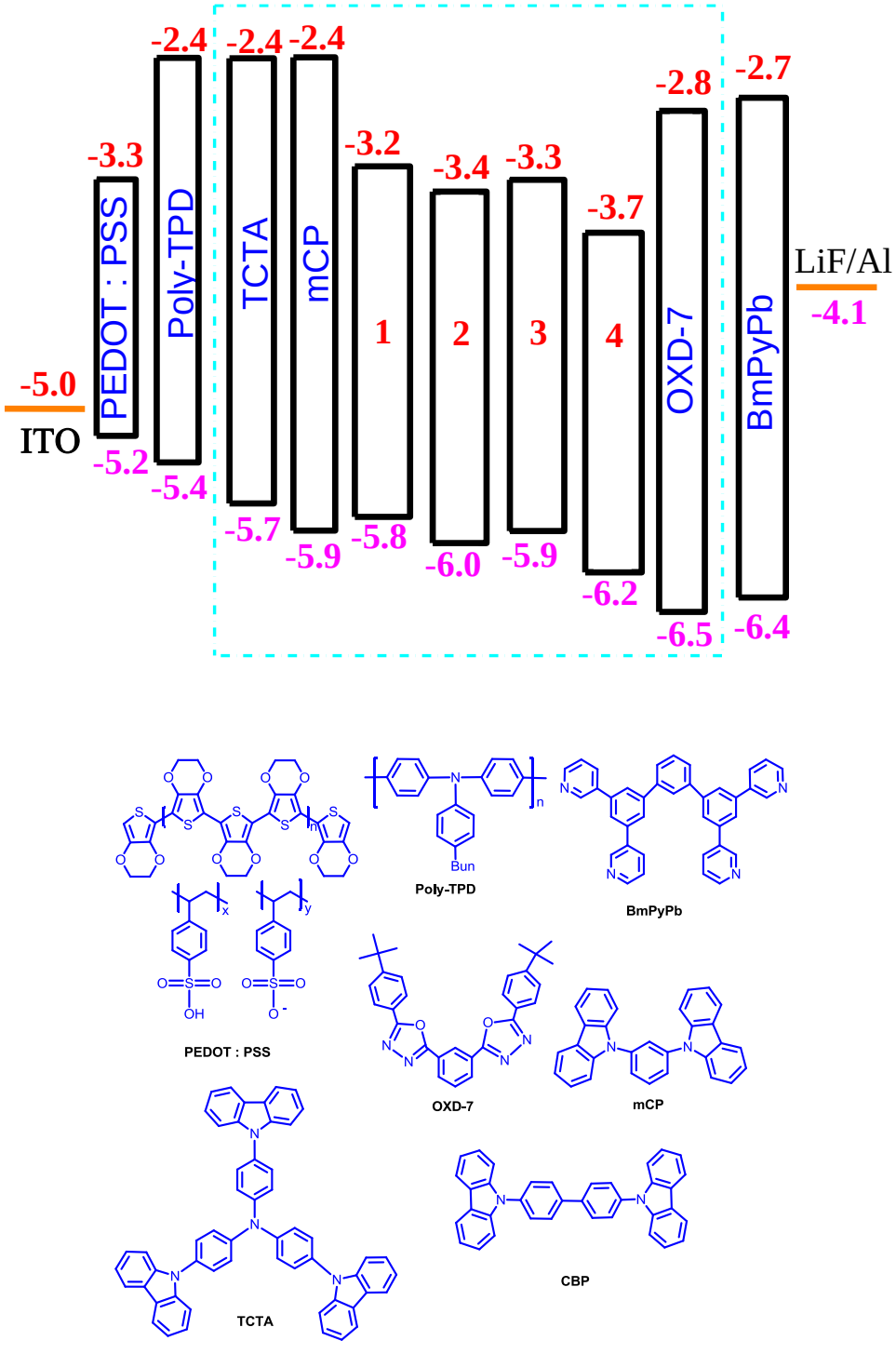

Figure S35. Energy-level diagrams of the transport and emitting materials together with organic materials used in devices.

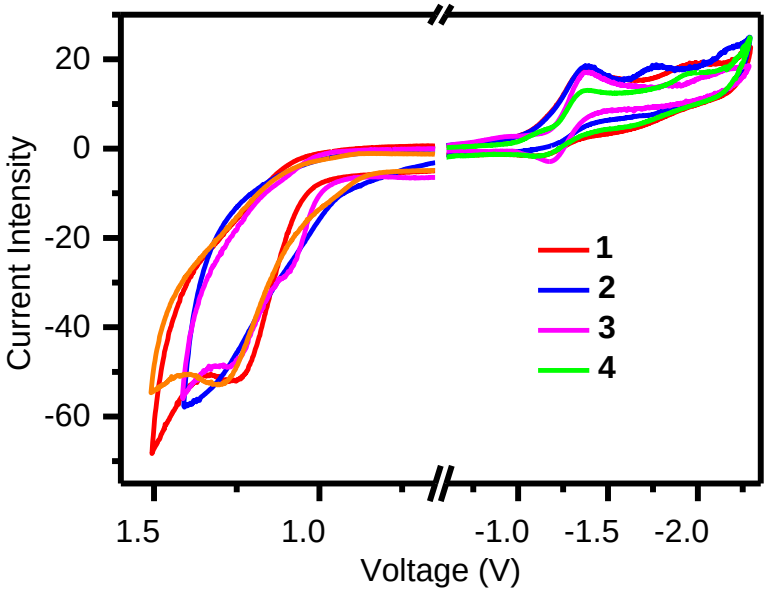

Figure S36. Cyclic voltammograms (reference to Fc/Fc^{+}) of complexes **1**–**4** in 0.1 M $(Bu_4N)(PF_6)$ acetonitrile solutions. The scan rate is 100 mV s^{-1}.

References

(1) Wang, Z.-Y.; Wang, J.-Y.; Zhang, L.-Y.; Yang, M.; Zhang, X.; Chen, Z.-N. Substituent Steric Effect Boosting Phosphorescence Efficiency of $PtCu_2$ Complexes. *J. Mater. Chem. C* **2020**, *8*, 5174–5182.

(2) Krause, L.; Herbst-Irmer, R.; Sheldrick, G. M.; Stalke, D. Comparison of silver and molybdenum microfocus X-ray sources for single-crystal structure determination. *J. Appl. Crystallogr.* **2015**, *48*, 3-10.

(3) Hubschle, C. B.; Sheldrick, G. M.; Dittrich, B. ShelXle: a Qt graphical user interface for SHELXL. *J. Appl. Crystallogr.* **2011**, *44*, 1281-1284.

(4) Frisch, M. J.; Trucks, G. W.; Schlegel, H. B.; Scuseria, G. E.; Robb, M. A.; Cheeseman, J. R.; Scalmani, G.; Barone, V.; Petersson, G. A.; Nakatsuji, H.; Li, X.; Caricato, M.; Marenich, A. V.; Bloino, J.; Janesko, B. G.; Gomperts, R.; Mennucci, B.; Hratchian, H. P.; Ortiz, J. V.; Izmaylov, A. F.; Sonnenberg, J. L.; Williams-Young, D.; Ding, F.; Lipparini, F.; Egidi, F.; Goings, J.; Peng, B.; Petrone, A.; Henderson, T.; Ranasinghe, D.; Zakrzewski, V. G.; Gao, J.;

Rega, N.; Zheng, G.; Liang, W.; Hada, M.; Ehara, M.; Toyota, K.; Fukuda, R.; Hasegawa, J.; Ishida, M.; Nakajima, T.; Honda, Y.; Kitao, O.; Nakai, H.; Vreven, T.; Throssell, K.; Montgomery, J. A., Jr.; Peralta, J. E.; Ogliaro, F.; Bearpark, M. J.; Heyd, J. J.; Brothers, E. N.; Kudin, K. N.; Staroverov, V. N.; Keith, T. A.; Kobayashi, R.; Normand, J.; Raghavachari, K.; Rendell, A. P.; Burant, J. C.; Iyengar, S. S.; Tomasi, J.; Cossi, M.; Millam, J. M.; Klene, M.; Adamo, C.; Cammi, R.; Ochterski, J. W.; Martin, R. L.; Morokuma, K.; Farkas, O.; Foresman, J. B.; Fox, D. J. Gaussian 16, Revision A.03. Gaussian, Inc., Wallingford CT, 2016.

(5) Perdew, J. P.; Burke, K.; Ernzerhof, M. Generalized Gradient Approximation Made Simple. *Phys. Rev. Lett.* **1996**, *77*, 3865–3868.

(6) Bauernschmitt, R.; Ahlrichs, R. Treatment of Electronic Excitations within the Adiabatic Approximation of Time Dependent Density Functional Theory. *Chem. Phys. Lett.* **1996**, *256*, 454-464.

(7) Casida, M. E.; Jamorski, C.; Casida, K. C.; Salahub, D. R. Molecular Excitation Energies to High-lying Bound States from Time-dependent Density-functional Response Theory: Characterization and Correction of the Time-dependent Local Density Approximation Ionization Threshold. *J. Chem. Phys*. **1998**, *108*, 4439-4449.

(8) Stratmann, R. E.; Scuseria, G. E.; Frisch, M. J. An Efficient Implementation of Time-dependent Density-functional Theory for the Calculation of Excitation Energies of Large Molecules. *J. Chem Phys*. **1998**, *109*, 8218-8224.

(9) Barone, V.; Cossi, M.; Tomasi, J. A New Definition of Cavities for the Computation of Solvation Free Energies by the Polarizable Continuum Model. *J. Chem. Phys.* **1997**, *107*, 3210-3221.

(10) Cossi, M.; Scalmani, G.; Rega, N.; Barone, V. New Developments in the Polarizable Continuum Model for Quantum Mechanical and Classical Calculations on Molecules in Solution. *J. Chem. Phys.* **2002**, *117*, 43-54.

(11) Andrae, D.; Häussermann, U.; Dolg, M.; Stoll, H.; Preuss, H. Energy-adjusted Ab initio Pseudopotentials for the Second and Third Row Transition Elements. *Theor. Chim. Acta*. **1990**, *77*, 123-141.

(12) Ros, P.; Schuit, G. C. A. Molecular Orbital Calculations on Copper Chloride Complexes. *Theo. Chim. Acta (Berl.)* **1966**, *4*, 1-12.

(13) Lu, T.; Chen, F. W. Multiwfn: A Multifunctional Wavefunction Analyzer. *J. Comp. Chem*. **2012**, *33*, 580-592.